Please cite this article in press as: Lee et al., The Development of Transparent Photovoltaics, Cell Reports Physical Science (2020), https://doi.org/10.1016/j.xcrp.2020.100143

Cell Reports
Physical Science

CellPress
OPEN ACCESS

Review

The Development of Transparent Photovoltaics

Kangmin Lee,[1] Han-Don Um,[1] Deokjae Choi,[1] Jeonghwan Park,[1] Namwoo Kim,[1] Hyungwoo Kim,[1] and Kwanyong Seo[1,*]

SUMMARY

Transparent photovoltaics (TPVs), which combine visible transparency and solar energy conversion, are being developed for applications in which conventional opaque solar cells are unlikely to be feasible, such as windows of buildings or vehicles. In this paper, we review recent progress in TPVs along with strategies that enable the transparency of conventional photovoltaics, including thin-film technology, selective light-transmission technology, and luminescent solar concentrator technology. From fundamental research to commercialization of the TPV, three main perspectives should be considered: (1) high-power conversion efficiency at the same average visible transmittance; (2) aesthetic factors, which should not detract from applications such as buildings and vehicles; and (3) feasibility for real-world applications, including modularization and stability evaluation. We present the distinct analysis criteria for these main perspectives and discuss their importance. We also discuss possible research directions for the commercialization of TPVs.

INTRODUCTION

Forty percent of the energy generated in the world is consumed in buildings, and, as industrialization advances, the portion of energy consumed in buildings is expected to increase.[1] Accordingly, the installation of energy conversion devices in buildings to produce energy from the building itself has been extensively studied. A representative example is solar panels on the exterior walls and roofs of buildings. However, as glass skyscrapers become increasingly common, the area of the exterior walls and roofs available for the installation of solar panels on such buildings is decreasing. In addition, the installation of conventional opaque solar panels on the exterior walls of buildings may detract from the original design of the building.[1] One of the measures to overcome these limitations is the development of transparent photovoltaics (TPVs). TPVs are expected to replace glass windows of buildings where conventional opaque photovoltaics (PVs) are unlikely to be applied directly, resulting in a significant increase in the area available for solar cells. Moreover, TPV technology expands the utilization of PVs because it can also be applied in various situations in which transparency is a requirement, including sunroofs and windows of vehicles and mobile devices.

The basic idea for the development of a TPV is to transmit a fraction of the incident light in the visible region that is recognized by human eyes. To implement this idea, representative strategies are classified into two types: (1) visible light absorption, in which light in the visible region is partially absorbed and transmitted;[2,3] and (2) luminescent solar concentrator (LSC) technology using luminescent materials.[4] The visible light-absorption-type TPV has been applied in most previous studies and mainly utilizes two typical technologies. Thin-film technology uses an ultrathin

[1]Department of Energy Engineering, Ulsan National Institute of Science and Technology (UNIST), Ulsan 44919, Korea

*Correspondence: kseo@unist.ac.kr

https://doi.org/10.1016/j.xcrp.2020.100143

Please cite this article in press as: Lee et al., The Development of Transparent Photovoltaics, Cell Reports Physical Science (2020), https://doi.org/10.1016/j.xcrp.2020.100143

light-absorption layer to allow the PVs to transmit a fraction of the incoming visible light. Selective light-transmission technology transmits visible light through selective light-transmission regions of the PV. The most developed TPV to date is the visible light-absorption type. As a result, some visible light-absorption-type TPVs currently reach a high-power conversion efficiency (PCE) of over 12% at an average visible transmittance (AVT) of 20%.[3,5] However, further research is required, such as modularization and scale-up of the unit cells (i.e., $\geq$ 5 inches) for practical application. The LSC-type TPV generates electricity by delivering the light emitted from luminescent materials embedded in a transparent substrate to opaque PVs located at the edge of the transparent substrate. Several studies have been conducted recently on LSC-type TPVs because they show high transmittance with a neutral color. The LSC-type TPV can exhibit high AVT values over 74% because they use luminescent materials that mainly absorb light in the ultraviolet (UV)/near-infrared (NIR) range.[6] In addition, large-area systems can be fabricated easily, because the size of the LSC-type TPV is determined only by the area of the transparent substrates in which the luminescent material is embedded. However, further research is required because the PCE values that have so far been reported for the LSC-type neutral-colored TPVs are low (up to 1.24% at an AVT of 74.4%).[6]

Although the development of TPV technology has been extensively investigated, the following challenges remain to be solved for practical use. First, the improvement of PCE is essential. In addition, a novel strategy is required to develop a neutral-colored TPV that does not detract from the aesthetics of the applications. High long-term stability, comparable to that of commercialized PVs, is also needed. In this review, we discuss key studies related to the development of neutral-colored TPVs with high PCE and high stability, based on the following questions:

(1) What are the key elements to consider when developing TPVs?
(2) What are the advantages and limitations of the techniques that have been applied to date to TPV development?
(3) What should be considered for the modularization of TPVs?
(4) What are the standard conditions to consider when evaluating the performance of the final device?

Finally, we discuss future works that are additionally considered for the practical application and commercialization of TPVs.

ESSENTIAL FACTORS TO CONSIDER IN TPV DEVELOPMENT

For the development of TPVs, the first step would be the selection of the appropriate light-absorbing material and device structure. In this step, for the ideal TPV fabrication, the three most important factors should be considered (Figure 1A): (1) high PCE at the same transmittance is required, and PCE must be maintained at all angles. (2) The TPVs should not detract from the aesthetics of applications. Therefore, the transmittance and color of the TPV need to be considered. Additionally, low haze ratio and maintenance of aesthetic factors at all angles are necessary considerations. (3) Long-term stability is required to commercialize TPVs.

First, PCE is an important factor denoting the performance of TPVs, similar to opaque PVs. In general, the higher light transmittance of TPVs leads to lower light absorption by the device, decreasing the PCE.[2] Consequently, TPVs show a relatively lower PCE compared with that of opaque PV with a transmittance of 0%. Therefore, for the development of highly efficient TPVs, it would be advantageous to study the

Please cite this article in press as: Lee et al., The Development of Transparent Photovoltaics, Cell Reports Physical Science (2020), https://doi.org/10.1016/j.xcrp.2020.100143

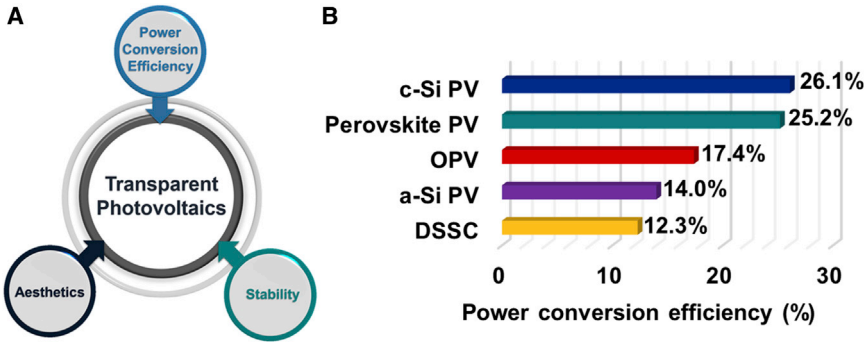

Figure 1. Main Key Elements to Consider When Developing TPV

(A) Three main factors to consider in the development of TPV.

(B) Best research-cell efficiency achieved to date (reference: National Renewable Energy Laboratory, Best Research-Cell Efficiency Chart).[7]

conventional PV technology that has recorded a high PCE of over 20% in an opaque form. This strategy has been confirmed through the recent research trends in the field of TPV technology.[3] Currently, for opaque PV, crystalline silicon (*c*-Si) and perovskite PVs exhibit a high PCE exceeding 25% (Figure 1B)[7] and this tendency is also observed in TPV research. While organic photovoltaic (OPV)-based and dye-sensitized solar cell (DSSC)-based TPVs show PCEs of approximately 5%–7% at a transmittance of 20%, *c*-Si-based and perovskite-based TPVs exhibit PCEs of over 12% at a similar transmittance.[3,5] When comparing and analyzing the PCEs of TPVs, the transmittance of the TPV must be considered along with the PCE as an important parameter because the PCE varies with the transmittance. Furthermore, the PCE measurement method must be optimized for the TPV and standardized to avoid the overestimation of the PCE by eliminating reflection or scattering from the backside of the PCE measurement systems. In addition, in a real environment, because the position of the sun varies with the day and year, the PCE values of TPVs also change with time. Therefore, to commercialize TPVs, a novel strategy is required to minimize PCE degradation due to the change in the angle of the incident light.

The second factor to consider is aesthetics. TPV technology aims to be applied where glass is used, including windows of buildings and vehicles. Thus, it is necessary to consider the transmittance and the color of TPVs. In addition, low haze ratio and maintenance of these aesthetic factors at all viewing angles are also necessary considerations. When considering the aesthetic factors for TPVs, it is challenging to directly compare those of hitherto-reported TPVs because the explicit criteria of the aesthetic elements for TPVs are presently unclear. The transmittance reported for TPV devices should represent the transmittance of the visible light range (380–780 nm), considering the response of the human eye to light. Therefore, AVT, which is the standardized average value of the transmittance in the visible wavelength range calculated by Equation 1, should be indicated for transmittance. The AVT of TPV can be determined by the ISO standard method (ISO 9050:2003) for PV, which is as follows:[8,9]

$$\tau_v = \frac{\sum_{380}^{780}(\tau) D_\lambda V(\lambda) \Delta\lambda}{\sum_{380}^{780} D_\lambda V(\lambda) \Delta\lambda} \quad \text{(Equation 1)}$$

where $\tau(\lambda)$ is the transmittance of the PV, D_λ is the spectral distribution of light incident on the PV, $V(\lambda)$ is the eye sensitivity factor, and $\Delta\lambda$ is the step size of the wavelength. As the required transmittance varies across the different fields of application,

at the fabrication stage, the transmittance of TPVs should systematically be tuned. Furthermore, the color of TPVs should be considered so as to not detract from the aesthetics of the target application. Accordingly, at the early stage of TPV research, experiments were conducted to adjust the color of pigments and organic matter to fabricate TPVs with various colors.[10] However, the possible application fields of colored TPVs are limited; studies to develop neutral-colored TPVs that look like bare glass are attracting considerable attention.[3,11] To precisely analyze the aesthetic elements, including transmittance and color, it is also necessary to consider the haze ratio that can confirm the degree of clearly visible transmitted light. In addition, for the color analysis of TPVs, the color rendering index (CRI) and the CIELAB color coordinate, which is specified by the International Commission on Illumination (CIE), should be considered for a clear comparative analysis.[12]

The third indispensable factor is long-term stability. Commercialized PVs require long-term use for more than 25 years.[13] Because TPVs would be a part of the target applications, the stability of TPV is more critical than that of the commercial opaque PV, which are independently installed on land or the rooftops of buildings. However, studies on TPVs have so far mainly focused on improving the PCE. Although some studies have recently reported on the improvement of the stability of organic PV,[14,15] further research is still required to improve the stability of organic-based PV;[16] this is because organic PV, such as DSSC and OPV, are still less stable compared with inorganic PVs, such as *c*-Si PV.[16,17] Perovskite PV, which have recently received tremendous attention, are also prone to stability issues such as moisture-induced degradation of the device and photo-instability.[18] Therefore, studies on the improvement of the stability of TPVs are essential. As stability evaluation is carried out after the encapsulation process using glass or ethylene vinyl acetate (EVA) film in actual applications, the assessment of the stability after the modularization process is more critical for commercialization.

Lastly, for commercialization, it is necessary to consider the fabrication cost of TPVs in addition to PCE, aesthetics, and stability. However, it is challenging to estimate the fabrication cost of TPVs accurately because most TPVs are not yet commercialized. The fabrication cost analysis has been reported in the case of conventional opaque PVs.[19-21] The estimation of the expected fabrication cost required for commercializing TPVs can be done by referring to the fabrication processes of opaque PVs. Additionally, it is necessary to consider the construction of the fabrication line for TPVs because it is essential to build a fabrication line for commercialization, and this cost is a significant part of the fabrication process. From this point of view, the *c*-Si-based TPVs have a substantial advantage because *c*-Si PVs, which dominate the market with a share of over 90%, already have an advanced fabrication line.

STRATEGIES FOR DEVELOPMENT OF TPVs

Visible Light-Absorption PV Technology

The visible light-absorption-type TPVs are PVs that partially transmit the visible light and absorb the remaining light to generate electricity. To impart transparency to PVs, transmission in the visible light region, which can be recognized by the human eye, is required. There are two main strategies for the development of visible light-absorption-type TPVs. The first is to fabricate a TPV via thin-film technology that partially transmits the visible light region by reducing the thickness of the light-absorbing layer. The second is the selective light-transmission technology, which is a method of transmitting visible light through selective regions of the device.

Please cite this article in press as: Lee et al., The Development of Transparent Photovoltaics, Cell Reports Physical Science (2020), https://doi.org/10.1016/j.xcrp.2020.100143

Thin Film Technology

The light-absorbing layer of a conventional solar cell mainly uses a material with a bandgap of 1.1–1.7 eV; thus, it absorbs visible light, making it opaque to the human eye.[22] However, reducing the thickness of the light-absorbing layer allows light transmission in the visible wavelength region, which can be described by the Beer-Lambert law (Equation 2).

$$I_T = I_0 \times e^{-\beta l} \quad \text{(Equation 2)}$$

where I_T, I_0, β, and l indicate transmitted light intensity, incident light intensity, absorption coefficient, and thickness of the absorbing layer, respectively. In other words, the light transmittance increases as the thickness of the light-absorbing layer decreases according to Equation 2. Therefore, thin-film technology is the most convenient method to fabricate TPVs, and it can be applied to typical light-absorbing films such as organic (polymer, dye),[23,24] inorganic (copper indium gallium selenide [CIGS], *a*-Si, CdTe, Quantum dot [QD]),[25-28] and perovskite[5,29] (Figures 2A–2H).

Figure 2I and Table 1 show the PCEs of the thin-film TPVs reported to date along with the AVT of the visible light region for each TPV.[2,5,24,25,28,29,31-56] In general, the PCE of a thin-film TPV decreases as the thickness of the light-absorbing layer decreases. By the Beer-Lambert law (Equation 2), light transmittance of the light-absorbing layer is exponentially inversely proportional to the thickness of the light-absorbing layer generating photo-induced carriers, which directly determine the PCE of the device as shown in Figure 2J. However, the light-transmittance characteristics of PV devices are quite different from those of the light-absorbing layer alone because, in the case of the PV devices, optical reflection and interference occur throughout the multi-layer structure of the device.[57] Therefore, it is necessary to understand the optical property profile of each layer to design optimized thin-film TPVs. Organic- and inorganic-based thin-film TPVs exhibit PCEs of up to 9.80% (with 38.3% AVT) and 9.78% (with 9.04% AVT), respectively (https://ubiquitous.energy/world-record/).[25] On the other hand, perovskite-based thin-film TPVs achieved a PCE of up to 12.6% at an AVT of 21.5%.[5]

To maintain transparency of the thin-film TPVs, transparent conducting electrodes (TCEs) are also required for both front and rear sides of the device, in addition to a transparent light-absorbing layer. The performance of the TCEs significantly affects the PCE of thin-film TPVs.[58] We generally consider two critical factors to design an ideal TCE for a high-efficiency thin-film TPVs: light transmittance and sheet resistance. The light transmittance of the conventional metal electrode is determined by the total surface area of the electrode that reflects the incident light, which is related to the optical shading loss; thus, we need to design the electrode to maximize transmittance. In addition, the sheet resistance of the electrode, which is particularly related to the current density and fill factor of the TPV, should be minimized to effectively collect photo-induced carriers generated in the light-absorbing layer.[58] Accordingly, as a strategy for high-efficiency thin-film TPVs, various studies have been reported on the development of TCEs focusing on high transmittance and low sheet resistance. The typical TCEs used primarily for the thin-film TPVs, so far, can be divided into those based on transparent conductive oxide (fluorine doped tin oxide, indium doped tin oxide),[21] carbon nanomaterials (graphene, carbon nanotube),[11,50] conductive polymers (poly(3,4-ethylenedioxythiophene) polystyrene sulfonate [PEDOT:PSS]),[56] and metal (ultrathin metal, metal nanowire, metal grid).[2,5,59-61]

Among these, carbon nanomaterial- and conductive polymer-based TCEs show a high sheet resistance (>60 Ω/sq) that is more than twice the sheet resistance (<30 Ω/sq) of metal-based TCEs at the same light transmittance (~90%)[62] Graphene has been mainly used as a TCE material in PV applications owing to the excellent

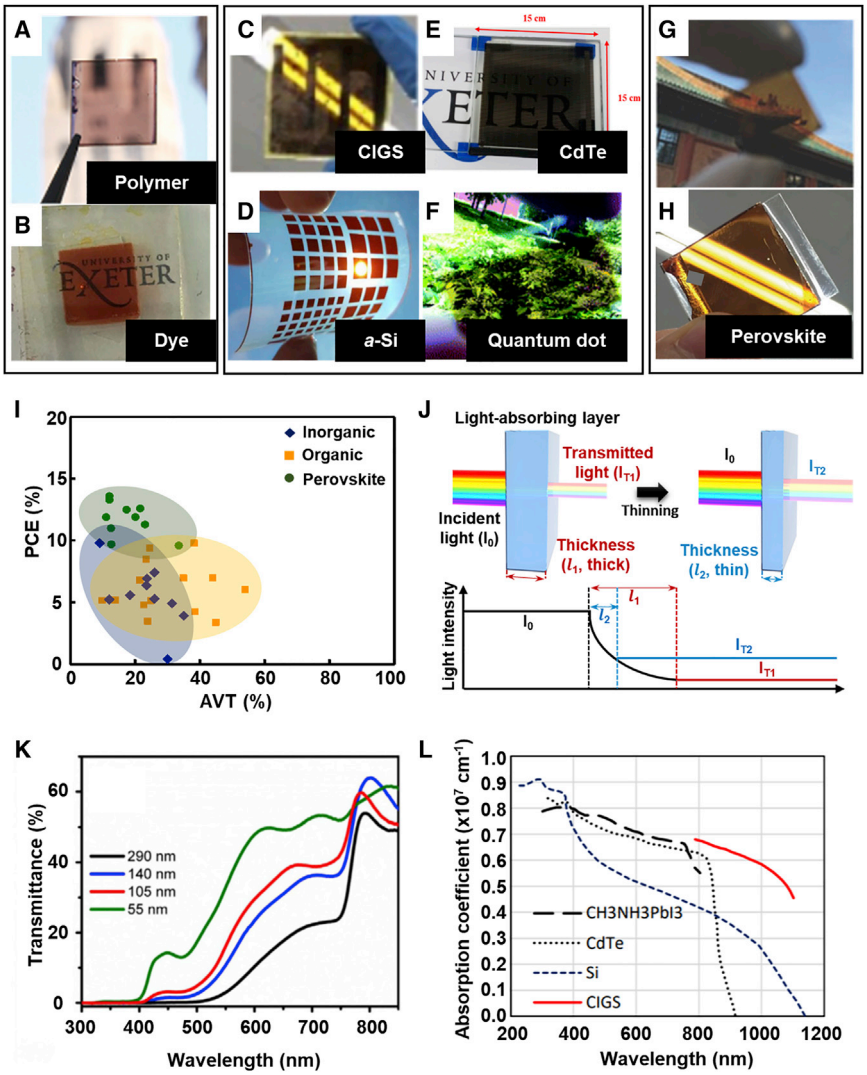

Figure 2. Photographs of Representative Thin Film TPV

(A) Organic polymer. Reprinted from Beiley et al.[23] with permission. Copyright 2013, Wiley-VCH.
(B) Organic dye[24] CC BY 4.0 license.
(C) CIGS. Reprinted from Shin et al.[25] with permission. Copyright 2019, Elsevier.
(D) Inorganic *a*-Si. Reprinted from Yang et al.[26] with permission. Copyright 2018, Elsevier.
(E) Inorganic CdTe. Reprinted from Alrashidi et al.[27] with permission. Copyright 2020, Elsevier.
(F) Inorganic QD. Reprinted from Zhang et al.[28] with permission. Copyright 2017, Royal Society of Chemistry.
(G) Perovskite. Reprinted from Xue et al.[5] with permission. Copyright 2017, Wiley-VCH.
(H) Perovskite. Reprinted from Heo et al.[29] with permission. Copyright 2015, Royal Society of Chemistry.
(I) PCE versus AVT for thin-film organic, inorganic, and perovskite TPV.
(J) Schematic illustration representing the relation of light transmittance to the thickness of light-absorbing layer.
(K) Transmittance spectra of complete perovskite TPV with different $CH_3NH_3PbI_3$ film thicknesses. Reprinted from Della Gaspera et al.[2] with permission. Copyright 2015, Elsevier.
(L) Absorption coefficient of various light-absorbing materials. Reprinted from Habibi et al.[30] with permission. Copyright 2016, Elsevier.

Please cite this article in press as: Lee et al., The Development of Transparent Photovoltaics, Cell Reports Physical Science (2020), https://doi.org/10.1016/j.xcrp.2020.100143

Table 1. Summary of the PCEs of the Thin Film TPV Reported to Date

Type	Material	AVT[a] (%)	PCE (%)	Reference
Inorganic	*a*-Si	23.5	6.36	31
	a-Si	23.6	6.92	32
	a-Si	12.0	5.20	33
	a-Si	18.4	5.57	34
	CIGS	9.04	9.78	25
	CIGS	26.0	5.27	35
	CdTe	30.0	0.41	36
	quantum dot	26.0	7.40	37
	quantum dot	31.4	4.90	28
Organic	polymer	21.6	6.83	38
	polymer	14.0	5.20	39
	polymer	38.6	4.27	40
	polymer	54.0	6.06	41
	polymer	45.0	3.40	42
	polymer	35.0	7.00	43
	polymer	22.8	4.81	44
	polymer	24.6	9.40	45
	polymer	44.0	7.00	46
	polymer	23.5	8.50	47
	polymer	38.3	9.80	https://ubiquitous.energy/world-record/
	dye	25.0	5.15	24
	dye	24.0	3.50	48
	dye	10.0	5.18	49
Perovskite	perovskite	12.6	9.70	50
	perovskite	33.4	9.60	51
	perovskite	16.0	11.8	52
	perovskite	17.3	12.5	29
	perovskite	16.0	10.1	2
	perovskite	21.5	12.6	5
	perovskite	11.0	11.9	53
	perovskite	20.0	11.9	54
	perovskite	12.5	11.0	55
	perovskite	23.0	11.3	56

[a]AVT is calculated based on data available in each reference.

chemical and thermal stability and mechanical robustness.[63] However, the thin-film TPVs using graphene TCEs showed a low PCE of 3.35% at an AVT of 40% with extremely low fill factor of 41.4%.[11] The low fill factor could result from the high sheet resistance (≈200 Ω/sq) of the graphene TCE due to defects and grain boundaries generated during the chemical vapor deposition (CVD) process.[11] Moreover, as a representative conducting polymer, PEDOT:PSS has been widely used for TPVs, which exhibited a PCE of 8.21% at an AVT of 23% with a low fill factor of 66%.[56]

In contrast, the thin-film TPV using metal-based TCEs has shown relatively high fill factor and PCE because of the high electrical conductivity (~10^7 S/m at 20°C) of

the metal itself.[64] Thus, metal-based TCEs have played a significant role in the improvement of the PCE of thin-film TPVs. The TPV using Ag thin film as a TCE showed a high fill factor of 76% through excellent carrier collection capability of the highly conductive TCE. Consequentially, the TPV with a Ag thin-film TCE achieved the highest PCE of 12.6% at an AVT of 21.5%.[5] In the case of a thin metal film TCE, however, there is an intrinsic limitation, in that light transmittance has a direct trade-off relation with the sheet resistance. The transparency of a metal film can be realized through ultra-thinning of an opaque metal, resulting in a significant increase in the sheet resistance. In contrast, metal nanowire and metal grid TCEs can be fabricated without controlling the thickness of the metal. Unlike metal thin film, these TCEs have the advantage of being able to achieve high AVT since they reserve a transparent region along with the specific metal region. Metal nanowire is a promising TCE material for PV because of both excellent conductivity and low-cost fabrication process. However, it also has critical drawbacks such as high junction resistance at the contact points between the metal nanowires and low electrical uniformity throughout the electrode network.[65] The thin-film TPV using Ag nanowire TCE achieved a PCE of 10.8% at an AVT of 25.5%, which is a higher PCE than that of a thin-film TPV with carbon nanomaterial TCEs. Unlike metal nanowire TCEs, metal grid TCEs provide a uniformly distributed metal network over the entire area of the TCEs and do not suffer from contact resistance.[61] Further, transmittance and sheet resistance can easily be controlled according to the grid spacing and width.[66] Owing to these advantages, research has been conducted on developing a TPV by applying a metal grid TCE with superior optical and electrical properties (i.e., $R_s \approx 25\ \Omega$/sq with over 97% AVT).[3]

Since thin-film technology enables PV to be made transparent by thinning the light-absorbing layer, it can be applied to all types of semiconducting materials without limitation. Previous research on thin-film TPV has been conducted with a focus on achieving high PCE using various materials. However, a TPV requires long-term stability and the appropriate aesthetics of a device along with a high PCE. Although organic and perovskite TPV exhibit relatively high PCE, these materials result in poor stability even in opaque PV because they exhibit intrinsic instability to water and oxygen.[16,18] In contrast, inorganic thin-film TPV are expected to show a relatively long-term stability owing to their outstanding stability to moisture and oxygen compared with organic and perovskite TPV. The light transmittance also varies according to the wavelength of the visible region because the absorption coefficient of the light-absorbing layer is different for different wavelengths (Figures 2K and 2L).[30] In general, the absorption coefficient of most light-absorbing materials tends to decrease toward the long-wavelength region. According to Equation 2, the thin-film TPV exhibits a relatively high light transmittance in the NIR region (~700 nm), resulting in a general reddish color (Figures 2A–2H).[2] Therefore, it is unlikely that the thin-film TPV would be a suitable candidate for applications that require a neutral color. In terms of fabrication cost, thin-film PV are known as low-cost PV because they can be fabricated easily via cost-effective processes such as evaporation, spin-coating, roll-to-roll, and screen printing[12] In addition, the material cost of thin-film TPV is expected to be lower than that of opaque PV, because the light-absorbing layer of thin-film TPV is much thinner than that of opaque PV.

SELECTIVE LIGHT-TRANSMISSION TECHNOLOGY

Another method to fabricate visible light-absorbing TPV is selective light-transmission technology. This method transmits light in the visible region through selective light-transmission regions. This strategy is frequently used to manufacture

Please cite this article in press as: Lee et al., The Development of Transparent Photovoltaics, Cell Reports Physical Science (2020), https://doi.org/10.1016/j.xcrp.2020.100143

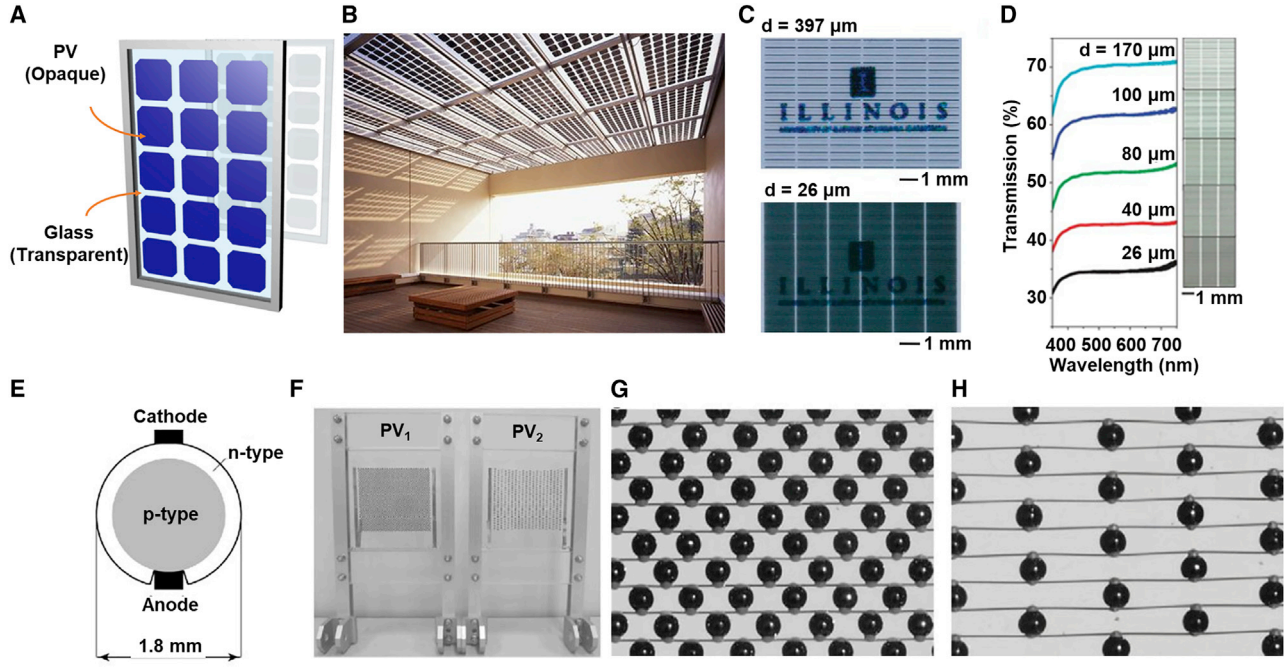

Figure 3. Light-Transmissive PV Modules

(A) Schematic of light-transmissive PV modules.

(B) Light-transmissive PV modules using *c*-Si PV. Reprinted from Peng et al.[67] with permission. Copyright 2011, Elsevier.

(C) Photograph of micro-sized PV arrays on PDMS (*d* is the spacing between two microcells).

(D) Transmittance of micro-sized PV arrays with spacing of 26, 40, 80, 100, and 170 μm. Reprinted from Yoon et al.[68] with permission. Copyright 2008, Nature Publishing Group.

(E) Schematic of the *c*-Si spherical PV.

(F–H) Light-transmissive PV modules (F) with cell density of (G) 15.4 cells/cm^2 (PV_1), and (H) 5.1 cells/cm^2 (PV_2). Reprinted from Yano et al.[69] CC BY 3.0.

light-transmissive PV modules for building-integrated PV (BIPV) systems.[1,67] As shown in Figures 3A and 3B, opaque PV are arranged with certain spacing on a transparent substrate such as glass, allowing them to exhibit light transmissivity through the transparent substrate region. While this method has the advantage of ease of manufacture, it has the critical drawback that all regions of the PV are opaque, thereby limiting the transmissive part and detracting from the aesthetics of the application.

To solve the issue that the installed PV significantly disturb the view, Yoon et al[68] developed a *c*-Si micro-sized PV cell with a length of 1.55 mm, a width of 50 μm, and a thickness of 15 μm and arranged them on a transparent substrate (10-μm-thick polydimethylsiloxane [PDMS]) to fabricate a light-transmissive mini-module (Figure 3C). The spacing between the PV was adjusted to tune the transmittance from 35% to 70% (Figure 3D). Using a similar approach, spherical *c*-Si PV with a diameter of 1.8 mm were fabricated and arranged on a 108 mm × 90 mm glass substrate to develop a light-transmissive mini-module (Figures 3E–3H)[69] The density of the PV in the glass substrate was adjusted between 5.1 and 15.4 cells/cm^2 to control the transmittance of the mini-module. Although the transmittance of these types of light-transmissive PV modules is somewhat tunable by changing the size of the opaque unit cell from the multi-centimeter scale to the millimeter scale, it is unlikely to define this mini-module as an ideal TPV because each unit cell is entirely opaque. Moreover, it does not satisfy the aesthetic factor because even the smallest unit cells are visible to the human eye.

Please cite this article in press as: Lee et al., The Development of Transparent Photovoltaics, Cell Reports Physical Science (2020), https://doi.org/10.1016/j.xcrp.2020.100143

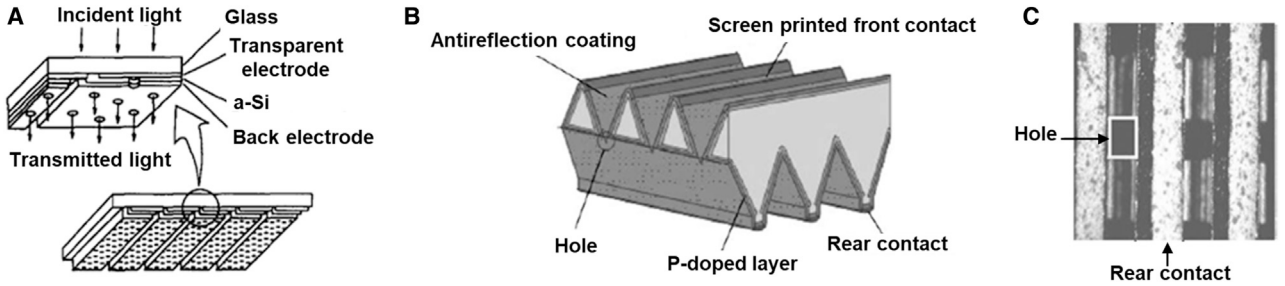

Figure 4. Development Methods of TPV by Forming an Aperture on the Active Layer of PV

(A) Schematic of see-through *a*-Si PV submodule. Reprinted from Takeoka et al.[70] Copyright 1993, Elsevier.

(B and C) Illustration of transparent POWER Si PV (B) and Photograph of the transparent POWER Si PV (C). Reprinted from Fath et al.[71] Copyright 2002, Elsevier.

Some research groups have tried to develop a TPV by forming an aperture on the active layer of a PV. For example, Sanyo Corp. developed see-through amorphous silicon (*a*-Si) PV in 1993 by forming apertures (with diameters of between 0.1 and 1.0 mm) on an *a*-Si PV (Figure 4A)[70] In the early 2000s, as shown in Figures 4B and 4C, the University of Konstanz reported the *c*-Si light-transmissive PV, which is called the transparent polycrystalline wafer engineering result (POWER) Si PV, by forming a tiny aperture in a certain area of the conventional *c*-Si PV[71] However, these PV were fabricated by forming apertures on conventional PV without considering the invisible conditions of apertures, resulting in opaque regions and apertures being inevitably recognized by the human eye. Therefore, these PV are not as transparent as glass; thus, it is difficult to replace glass with these PV and they continue to detract from the aesthetics of the application.

Recently, the Seo group developed a neutral-colored TPV[3] To that end, they attempted to fabricate a transparent *c*-Si wafer, which is the primary material of a *c*-Si PV. First, the size of the light-transmission window (LTW) was designed so that all visible wavelengths can be completely transmitted through the LTW. The spacing between the LTWs was designed by considering the minimum angle of resolution for the human eye to make individual LTWs invisible to the human eye[72] Consequently, the transparent *c*-Si substrate shows a neutral color without a transmission cut-on wavelength (right in Figure 5A), even though it has the same thickness as a commercial *c*-Si wafer (left in Figure 5A). Furthermore, the transmittance of the substrate is systematically tunable by controlling the size and spacing of the LTWs (Figures 5B and 5C) while maintaining a neutral color (Figure 5D). In addition, as shown in Figure 5E, the transparent *c*-Si substrates showed a low haze ratio (0.95%), similar to that of glass (0.89%). The TPV based on the transparent *c*-Si substrate exhibited a very high PCE of up to 12.2% (AVT of 20%) while maintaining its neutral color (Figure 5F). Thus, the transparent *c*-Si TPV would be advantageous when used as BIPV because of the angle-dependent transmittance of the devices (Figure 5G). Moreover, as this TPV was fabricated with the same structure as commercial *c*-Si PV, similarly high stability is expected. Furthermore, it is expected that rapid commercialization of the *c*-Si TPV would be possible because the fabrication process of the *c*-Si TPV is similar to that of commercialized *c*-Si PV, except for the etching step. In addition, if the wet etching technique is applied to fabricate the LTWs of the *c*-Si TPV, the fabrication cost of the *c*-Si TPV is expected to be similar to that of commercialized *c*-Si PV.

LSC PV TECHNOLOGY

For a high level of transparency in the visible wavelength region, various studies have investigated the generation of electricity by absorbing only UV (<380 nm) and NIR

Please cite this article in press as: Lee et al., The Development of Transparent Photovoltaics, Cell Reports Physical Science (2020), https://doi.org/10.1016/j.xcrp.2020.100143

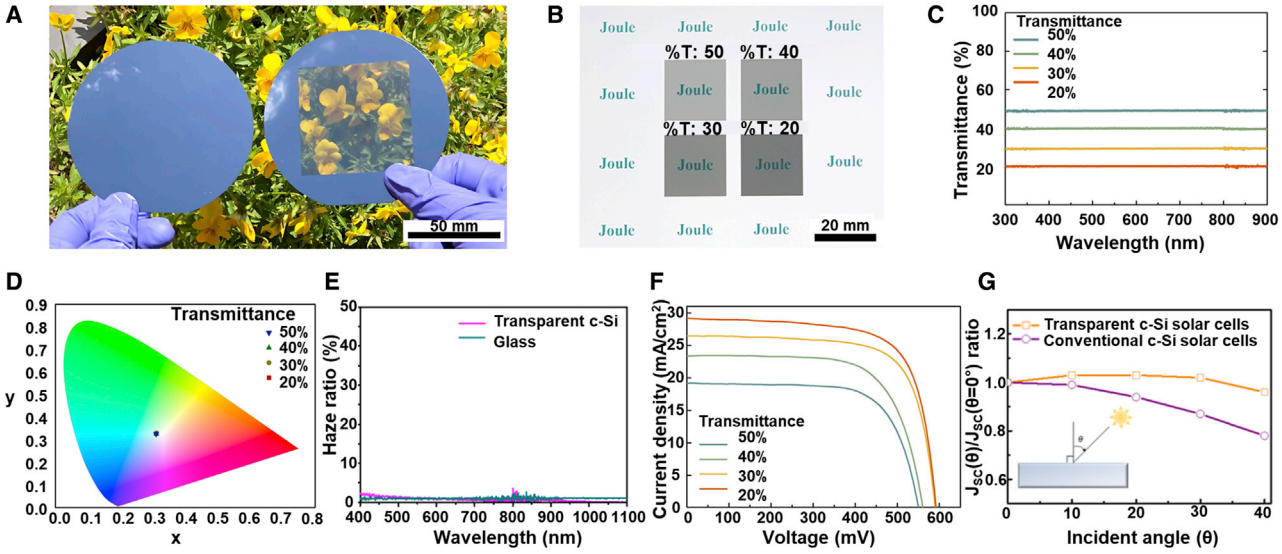

Figure 5. Neutral-Colored *c*-Si TPV

(A) Photograph of a 200-μm-thick conventional polished *c*-Si wafer (left) and a neutral-color transparent *c*-Si substrate at the center of the conventional *c*-Si wafer (right).

(B and C) Photograph of transparent *c*-Si substrates with different transmittance (B) and total transmittance spectra (C).

(D) Representation of the color coordinates of the *c*-Si TPV with different transmittances on the CIE 1931 chromaticity diagram.

(E) Transmission haze ratio of the *c*-Si and bare glass.

(F) *J–V* characteristics of *c*-Si TPV.

(G) Relative photocurrent for different light incidence angles, with respect to photocurrent at normal incidence of the transparent *c*-Si TPV and conventional *c*-Si solar cells. Reprinted from Lee et al.[3] Copyright 2020, Elsevier.

(>780 nm) parts of the solar spectrum, which are not visible to the human eye. OPVs and DSSC TPVs have been developed in an attempt to demonstrate TPV with a neutral color like glass using semiconducting organic materials that selectively absorb light in the UV or NIR region[73-78] However, most solar cells reported to date absorb a significant amount of visible light through not only semiconducting materials but also other layers such as the hole transport layer (HTL), electron transport layer (ETL), and TCEs[79-81] Consequently, the PV revealed a low AVT of 10%–70% that limits neither visible light transmission nor demonstrating a neutral color[82-85]

In contrast, LSC-type TPV technologies employ luminescent materials that absorb and emit light in the UV/NIR region. Very high AVTs over 74% have been reported for LSC-type TPV[6] The luminescent materials embedded in a transparent polymer substrate absorb UV or NIR photons and simultaneously emit light of longer wavelength, in general, than that of the absorbed light[86] This process can be understood to be similar to the energy downshifting of light[87] The emitted light from the luminescent material is guided to the edge of the transparent polymer substrate, where conventional opaque PV are installed in the form of thin strips (Figure 6A). The waveguiding of the emitted photons is attributed to the total internal reflection due to the refractive index difference between the polymer and air. In turn, the LSC comprises two parts: a light-absorbing area that includes the luminescent materials and a conventional PV area that produces electricity. Because the edge area is visibly negligible, the LSC-type TPV has the advantage of being able to realize perfect transparency with almost no absorption of visible light, like glass (Figure 6B). *c*-Si, GaAs, and InGaP PV have mainly been used as edge PV and organic dyes and QDs are commonly used as the luminescent materials embedded in transparent

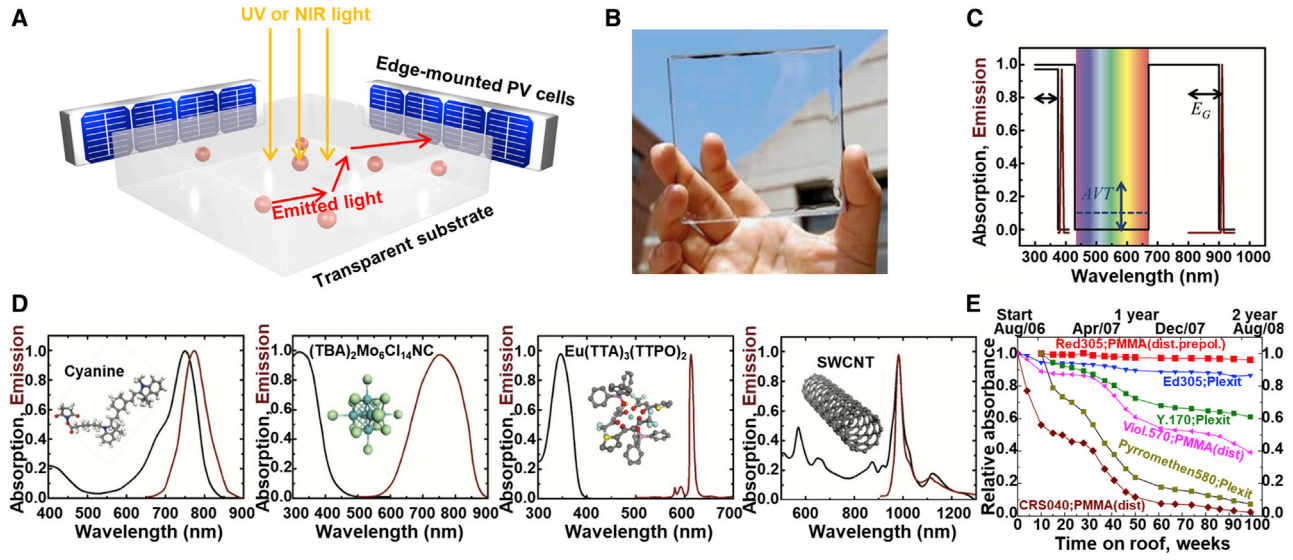

Figure 6. LSC-Type TPV

(A and B) Schematic (A) and representative (B) photograph showing the LSC-type TPV technology. Reprinted from Zhao et al.[4] Copyright 2014, Wiley.

(C) Schematic of absorption and emission characteristics of ideal luminescent material. Reprinted from Yang et al.[86] Copyright 2017, Wiley.

(D) Representative absorption and emission spectra (normalized) of typical luminescent materials applied in LSC-type TPV. Reprinted from Yang et al.[86] Copyright 2017, Wiley.

(E) Relative absorbances in band maxima as a function of time of out-door storage and polymer matrix[88] CC BY 4.0 license.

polymer substrates[89,90] In addition, the LSC technology would be more facile than other TPV strategies for implementation in a large area system by an inexpensive process[91] The size of the LSC is determined by the area of the transparent polymer substrate that includes the luminescent material. The transparent polymer substrate with luminescent material can be fabricated at a large scale using inexpensive methods such as casting, coating, and roll-to-roll processes[89,92] Additionally, the solar cell installed at the edge of the LSC has already been commercialized at large scales. Consequently, large-scale LSCs have been demonstrated with a size of over 100 cm^2 via a cost-effective method[89,93] Thus, LSC-type TPV technology has strengths for BIPV or vehicle-integrated PV (VIPV) applications that require that TPV replace a large scale of a glass substrate.

Table 2 summarizes the optical power efficiency (OPE), PCE, AVT, size, and type of solar cells installed at the edge of the LSCs[4,6,94–97] It is necessary to carefully distinguish the OPE and PCE when referring to previous studies. OPE is the energy ratio of the light emitted by a luminescent material to the energy of incident light from the sun (AM 1.5G solar spectrum). PCE can be estimated by the equation PCE = OPE × η_{PV}, where η_{PV} is the PCE of the edge-mounted PV[91] The OPE varies according to the actual LSC size because of the energy loss due to various reasons such as the escape of emitted light from the transparent polymer substrate before being guided to the target solar cells[88,98] From this perspective, the actual size of the LSC should be considered one of the main parameters for the evaluation of the device. The LSC-type TPV technology has demonstrated lower OPE and PCE than those of other strategies. In particular, the reported efficiency is considerably lower than the theoretical efficiency, because current technology is far from the ideal condition. We can consider the following requirements for the ideal LSC-type TPV strategy: (1) the luminescent material absorbs almost 100% of UV/NIR light that is in the possible absorption range; (2) the photoluminescence (PL) efficiency is 100%; (3) the emitted photon must reach the edge-mounted PV without any losses; (4) the efficiency of

Table 2. Summary of the Characteristics of Transparent Luminescent Solar Concentrator

Luminescent Material	OPE (%)	PCE (%)	AVT (%)	Active Area (cm^2)	Thickness (cm)	Mounted PV
Metal halide[94]	–	0.44	84	6.25	0.1	*c*-Si PV
CY[4]	–	0.4	86	4	0.1	*c*-Si PV
Cy7-CA[95]	–	0.3	87.7	25.8	0.1	*c*-Si PV
gem-Pyrene Ethenes[96]	2.1	0.32	N/A	6.25	0.1	*c*-Si PV
EuTT[97]	–	0.28	N/A	100	0.3	*c*-Si PV
Cy7-NHS[6]	–	1.24	74.4	25.8	0.635	GaAs PV

OPE, optical power efficiency; PCE, power conversion efficiency; AVT, average visible transmittance; PV, photovoltaics.

the edge-mounted PV is close to the Shockley-Queisser limit (33.1%); and (5) there is no optical loss in the transparent polymer substrate due to reflection or transmission.

The dominant reason for low PCE of the LSC-type TPV technology is the low OPE of the luminescent materials. Figure 6C shows the absorption and emission spectra of the ideal luminescent material. The ideal luminescent material absorbs 100% of the UV/NIR light in the possible absorption range while allowing 100% transmittance of visible light. In contrast, typical luminescent materials applied in LSC (Figure 6D) have significantly lower absorption of light in the UV/NIR region, which results in a reduced number of photons reaching the edge-mounted PV, causing low OPE of the LSC. Therefore, the light-absorption capability of the luminescent materials in the UV/NIR region must be improved to increase the OPE. To improve the UV/NIR light absorption, various types of luminescent material have been explored, such as core/shell structured QDs[99] nanocrystal[100,101] and rare-earth ion complexes[97,102] However, further research is required.

Figure 6C also shows that the ideal absorption and emission spectra do not overlap. When the two spectra overlap, the emitted photon can be reabsorbed by luminescent material. Such a re-absorption loss reduces the OPE of the LSC, and the OPE of LSC rapidly decreases as the area of the LSC increases due to the enhanced re-absorption loss. Thus, the minimization of the spectral overlap of absorption and emission in LSC would be a direct solution to reduce the re-absorption loss of emitted photons in the polymer matrix[98] This could be achieved by reducing the bandwidth of the emission spectrum and also by increasing the Stokes shift, which is the difference between the positions of the band maxima of the absorption and emission spectra. The tunability of absorption and emission spectra has been demonstrated by controlling the reaction conditions, particle sizes, molecular structures, and compositions of the luminescent materials[86,103,104]

The lifetime of the LSC-type TPV mainly depends on the stability of the luminescent materials. This is because other components of the LSC-type TPV, the transparent polymer and edge-mounted PV (e.g., *c*-Si PV), have exhibited long lifetimes of several years or more. The stability of luminescent materials should be evaluated after embedding in a transparent polymer substrate in the same manner as the actual LSC structure. Figure 6E shows the lifespan of luminescent organic dyes commonly used in LSC. Examining the change in absorbance of the dye embedded in the transparent polymer substrate reveals that few materials are relatively stable throughout the period of 2 years. Such a low stability is attributed to the fact that most luminescent materials are sensitive to oxygen and moisture under atmospheric condition,

Please cite this article in press as: Lee et al., The Development of Transparent Photovoltaics, Cell Reports Physical Science (2020), https://doi.org/10.1016/j.xcrp.2020.100143

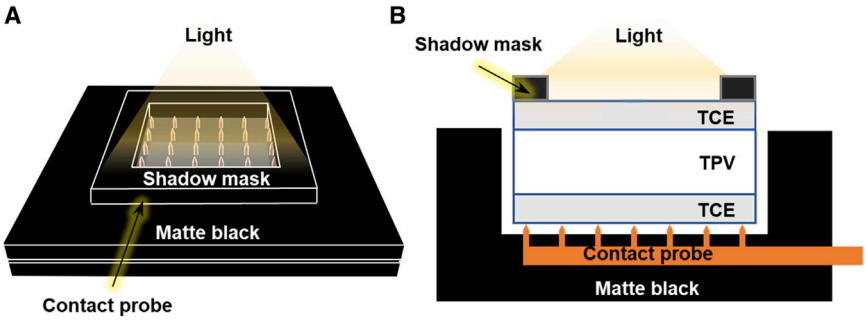

Figure 7. Schematic of a PCE Measurement System with Matte Black Background and a New Type of Bottom Contact Probe

(A) Three-dimensional (3D) schematic of the PCE measurement system.

(B) Cross-sectional schematic of the PCE measurement system.

resulting in a short lifetime[88] Thus, efficient encapsulation strategies against moisture and oxygen are required[91,105] Moreover, there is no standard for the stability evaluation of LSC-type TPV. Therefore, it is necessary to provide the specific lifetime of LSC-type TPV and also to establish a standard stability test.

STANDARD CRITERIA FOR ANALYSIS OF TPV

To accurately evaluate whether fabricated TPV satisfy the aforementioned essential elements, it is necessary to define explicit standards regarding the analysis criteria. We discuss here how to evaluate the performance and aesthetic factors of TPV. In addition, the possible modularization and stability evaluation of TPV will be described with reference to the industrial standards for conventional PV.

Performance Evaluation of TPV

The PV performance of a TPV can be evaluated as the ratio of the energy input to the energy output, which is the same as the measurement in a conventional PV and can be defined by the following equation[106]

$$\mathrm{PCE} = \frac{P_{out}}{P_{in}} = \frac{V_{oc} \times J_{sc} \times FF}{P_{in}} \qquad \text{(Equation 3)}$$

where V_{oc} is the open-circuit voltage, J_{sc} is the short-circuit current, and FF is the fill factor. The standard measurement is performed under simulated AM 1.5G solar illumination at a temperature of 25°C. TPV are intentionally designed to transmit light in a specific range of wavelengths in the solar spectrum, while conventional PV are designed to minimize the reflection and transmission of light to increase the PCE. When measuring the PCE of a TPV, in particular, the J_{sc} may be overestimated if the transmitted light is re-absorbed. In the conventional PCE measurement system, the stage for PV is made of metal for easy contact with the rear side of the PV. Since TPV mainly use TCEs on the rear side, there is a possibility that the transmitted light is reflected back to the TPV by the metal plate on the stage. Thus, it is necessary to prevent the reflection of the transmitted light from the bottom stage. One way to do this is to place a matte black background between the TPV and the metal stage of the setup[107] In addition, modified bottom contact probes are required to enable ohmic contact between the TPV and PCE measurement systems, as shown in Figure 7.

Additionally, for accurate J_{sc} measurements of TPV, the calculated J_{sc} value from external quantum efficiency (EQE) should be compared with the measured J_{sc} value. The EQE spectrum represents the light collection capability of a PV according to the wavelength of incident light. It is defined as the ratio of the number of collected

Please cite this article in press as: Lee et al., The Development of Transparent Photovoltaics, Cell Reports Physical Science (2020), https://doi.org/10.1016/j.xcrp.2020.100143

charge carriers to the number of photons incident at specific wavelengths, as shown in Equation 4[108]

$$EQE = \frac{electrons.s^{-1}}{photons.s^{-1}} = \frac{current/e}{total\ photon\ power/h\nu} \quad \text{(Equation 4)}$$

The efficiency of carrier collection of a TPV according to the wavelength of incident light can be evaluated through the EQE measurement. The J_{sc} calculated from EQE can be obtained according to Equation 5[109]

$$J_{sc} = e \cdot \int EQE(\lambda) \cdot AM1.5G(\lambda) d\lambda \quad \text{(Equation 5)}$$

where e and λ represent the elementary charge and wavelength, respectively. Here, we can confirm whether the measured J_{sc} is accurate compared with the J_{sc} value calculated from the EQE. In a previous survey of erroneous efficiency reports for PV, approximately 37% of the PV literature reports overestimated J_{sc} and PCE values[110] To ensure a reliable performance check of a TPV, the calculated J_{sc} value from the EQE spectrum should be reported along with the measured J_{sc} value.

In addition, it is necessary to consider the AVT when measuring the PCE of TPV. The Lunt group proposed the concept of light utilization efficiency (LUE), represented as the product of AVT and PCE values, as the criterion for evaluating the efficiency of TPV relating to the AVT[91] The LUE value can be used as a convenient figure of merit to compare the performance of TPV, but, when only the LUE value is presented, information about the AVT and the PCE of the TPV is veiled. Therefore, both AVT and PCE should be simultaneously indicated as figures of merit for comparing the PV performance of TPV.

ASSESSMENT OF THE AESTHETICS OF TPV

The figures of merit for the analysis of the aesthetic factors of TPV include standardized transmittance, transmission haze ratio, CRI, and CIELAB color coordinates. The first figure of merit regarding the aesthetics of TPV is transmittance. Currently, the transmittance of TPV has been presented in various ways because the transmittance of TPV has no specific evaluation standard. AVT is the standardized average value of the transmittance in the wavelength range of 380–780 nm, which is visible to the human eye.

Second, the transmission haze ratio should also be measured. The transmission haze ratio can be estimated as the ratio of the diffuse transmittance (T_d) to the total transmittance (T_t)[111]

$$H(\%) = \frac{T_d}{T_t} \times 100 \quad \text{(Equation 6)}$$

Transmission haze ratio is a measure of the degree to which light passing through a TPV is scattered or reflected, causing objects located on the back of the solar cell to be blurred. The lower the value of the transmission haze ratio, the clearer the object located on the back of the TPV. Therefore, it is necessary to develop a TPV with a low transmission haze ratio, and it is also essential to compare the transmission haze ratio of glass ($\lesssim$1%) currently used in the window field[111]

The aesthetic factors of TPV to be considered along with the values of AVT and transmission haze ratio are the CRI and the CIELAB color coordinates, which are the figures of merit that indicate the color rendering and the presence or absence of color. These values are measured under the same standard light source (AM 1.5G) as those

Please cite this article in press as: Lee et al., The Development of Transparent Photovoltaics, Cell Reports Physical Science (2020), https://doi.org/10.1016/j.xcrp.2020.100143

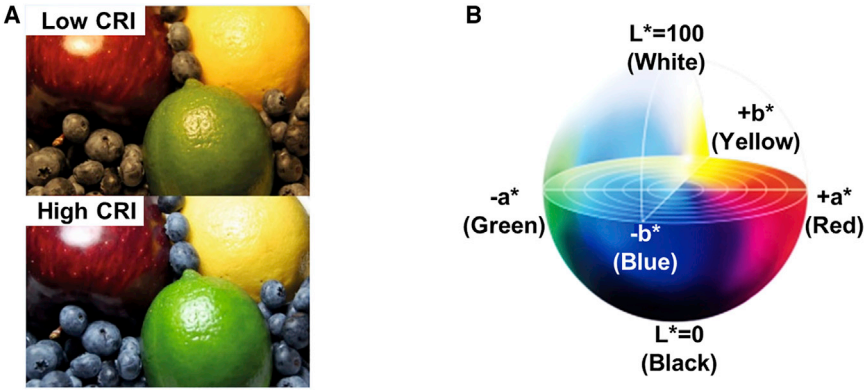

Figure 8. Assessment of the Aesthetics of TPV

(A) Comparison of a low and high CRI. Reprinted from Traverse et al.[91] with permission. Copyright 2017, Nature Publishing Group.

(B) Illustration of CIELAB color space. Reprinted from Tang et al.[112] CC BY-NC-ND 4.0.

used for PV performance measurement. The CRI is the quantitative value of color-rendering capacity estimated by comparing the color of an object seen through a TPV with the original color under the reference illumination source[12] CRI ranges from 0 to 100, where a higher CRI value represents a better color rendering (Figure 8A)[91] A high value of the CRI close to 100 indicates that the color of an object seen through the TPV is almost identical to the original color[12] CRI is either obtained by direct measurement using color-measuring equipment such as a colorimeter or by calculating the CRI value from transmittance data of the TPV[57,113]

Another color standard to evaluate the aesthetics of TPV is the CIELAB color coordinates, which is a system suggested by the CIE that depicts the color of an object using three coordinates (Figure 8B). In general, CIE chromaticity diagrams, such as CIE 1931 xy and CIE 1971 uv, have mainly been used for evaluating the color of TPV[3,5,10,11,74] However, some colors that differ only in brightness, such as white and gray, cannot be distinguished in the CIE chromaticity diagram[3] In contrast, CIELAB color coordinates can display both chromaticity and brightness values. As shown in Figure 8B, the L* value represents brightness from black (0) to white (100)[112] The a* value indicates green to red, and the b* value shows blue to yellow. When the values of a* and b* are closer to 0, the color is more neutral. The color coordinates of a TPV can be easily obtained by using color measurement instruments such as a color spectrophotometer. The color of the TPV can be clearly confirmed through the measurement of the CIELAB coordinates, and this would be an excellent way to check how close the TPV is to a neutral color. Accordingly, CRI and CIELAB color coordinates should be considered for the accurate evaluation of the aesthetics of TPV, which can be used as a figure of merit to determine the possible applications of developed TPV.

MODULARIZATION AND STABILITY EVALUATION OF TPV

In addition to the aforementioned factors, PCE and aesthetics, research on modularization and stability is also required for the commercialization of TPV. A 6-inch *c*-Si PV generates power of approximately 2–5 W with a voltage of approximately 0.5–0.6 V and a current of 4–8 A[7] For practical applications such as operating systems or power plants; however, PV modules should be designed to produce appropriate currents and voltages, which are generally much larger than those of a single unit device. In addition to designing for suitable power, the modularization of PV is critical for improving the stability of the PV through the encapsulation of the module.

Please cite this article in press as: Lee et al., The Development of Transparent Photovoltaics, Cell Reports Physical Science (2020), https://doi.org/10.1016/j.xcrp.2020.100143

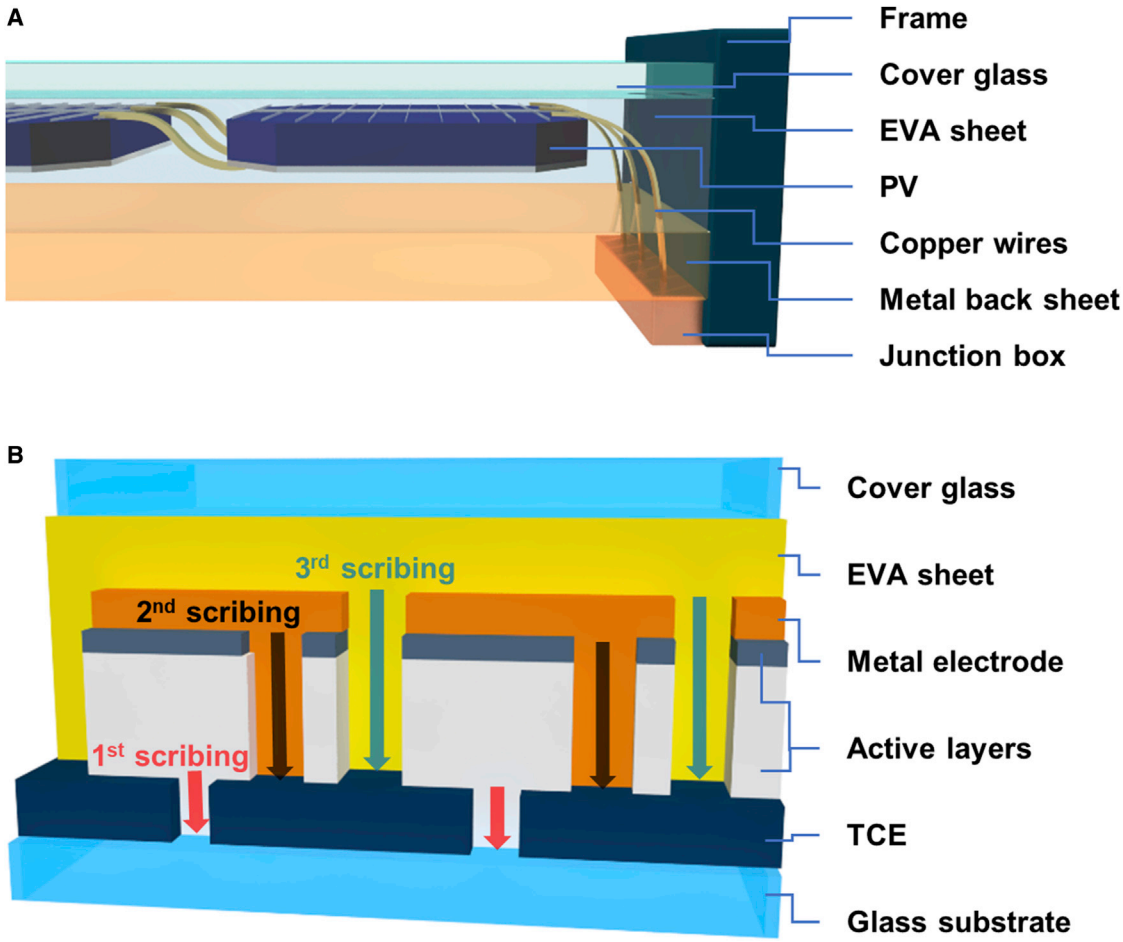

Figure 9. Modularization of PV

(A) Schematic of *c*-Si PV module.

(B) Modularization schematic of thin-film PV module fabricated by laser scribing.

The modularization process of PV can be categorized based on the type of PV: (1) wafer-based PV such as *c*-Si and (2) thin-film PV formed by coating on a glass substrate such as organic PV and perovskite PV. Since metal electrodes exist on both the front and rear surfaces of *c*-Si PV, the rear electrode would be connected to the top electrode of neighboring cell to connect each in series. For commercial *c*-Si PV modules, tinned copper flat wires are used as a solder wire to interconnect two unit cells in series or in parallel as shown in Figure 9A. Owing to the physical gap required for interconnection between the unit cells, some areal loss of the solar module is unavoidable, leading to the degradation of the module efficiency compared with the PCE of the unit PV (Chung et al., 2012, 38th IEEE Photovoltaic Specialists Conference). In addition, because of the large width (1–6 mm) of the copper wire,[114] the interconnections of the copper wires on the solar module are inevitably visible, which deteriorates the aesthetics of TPV modules. Accordingly, rather than the conventional *c*-Si PV structure with electrodes located on both the front and rear sides, an interdigitated back contact (IBC) PV with all the electrodes on the rear surface would be considered[115] The IBC PV would not require the large space between the PV because of a relatively simple interconnection between two unit cells on the same side. Because of a narrow gap less than hundreds of micrometers between the cells, the PV could be interconnected with fine copper wire rather than

Please cite this article in press as: Lee et al., The Development of Transparent Photovoltaics, Cell Reports Physical Science (2020), https://doi.org/10.1016/j.xcrp.2020.100143

conventional copper wire with a width of 1–6 mm. IBC-based modularization with fine copper wire connections may be an appropriate approach to ensure the aesthetics requirement of the TPV module.

As shown in Figure 9A, the conventional *c*-Si PV module consists of cover glass on the front side, a polymer sheet bonded to the front and rear sides to protect the module, and a metal back sheet located on the rear side of the module. In general, 3.2-mm-thick soda-lime glass is used as the cover glass (Kambe et al., 2013, IEEE 39th Photovoltaic Specialists Conference). For the standardized size of a solar module (1600 × 980 mm^2), the weight of the cover glass is approximately 12–13 kg, which is more than 60% of the total weight of the module. The polymer sheet directly covering the PV module is EVA. The EVA film exhibits rubber-like material properties in flexibility and softness[116] Furthermore, EVA is transparent and resistant to damage from stress-cracking, UV radiation, and extreme temperature conditions (−40/80°C)[117] For the TPV module, instead of an opaque aluminum back sheet, glass should be used on the rear side to form a glass-to-glass-type module structure, resulting in a significant increase in the weight of the module. Therefore, it is necessary to develop polymer-based materials that can replace the cover glass to achieve both the low weight and high stability of the conventional solar module for TPV modules.

The modularization process of thin-film PV fabricated on a glass substrate (e.g., an organic PV or a perovskite PV) is intrinsically different from that of the wafer-based *c*-Si PV. Figure 9B presents a schematic of the modularization processes for thin-film PV modules, which is performed by a laser and mechanical scriber to isolate a TCE/light absorber/metal electrode. The TCE coated onto the entire glass substrate is patterned by the first scribing, followed by coating the active layers onto the patterned TCE. Then, the active layers are patterned by the second scribing. Finally, the metal electrode is deposited onto the patterned active layers, followed by the third scribing to isolate the metal electrode. By selectively patterning the layers of the PV, the cells are isolated and interconnected in series with neighboring cells. Because of precise laser scribing, it is possible to minimize the areal loss during the modularization. After laser scribing, the patterned layers are filled with the EVA film. The module fabrication is completed by covering the top of the EVA film with the cover glass. Since the TPV use TCE as front and rear electrodes instead of metal electrodes, the series resistance would be considerably higher than that of the conventional thin-film PV with metal electrodes. Currently, a metal electrode would be essential to prevent resistive and power losses for the large scale of commercial modules. To avoid deterioration of the aesthetics, an appropriate electrode design for the TPV module is also required.

Another key purpose of modularization is to protect PV from the environment. Recent reports of TPV have focused on improving PCE and transparency. However, not much discussion has been reported regarding standardized methods for evaluating the stability of the TPV module. Thus, based on the typical methods for assessing the stability of a commercial PV module, it is also beneficial to discuss the requirements for commercializing the TPV module. The ideal PV module, suitable for many applications from solar power plants to BIPV systems, requires a service lifetime of more than 25 years. Since it is unrealistic to monitor the performance of the installed solar module under outdoor conditions for decades, an accelerated stress test has been developed to measure the long-term performance of a PV module in a short time. The international electrotechnical commission (IEC) 61646 certification was proposed mainly for the *a*-Si PV module[89] However, recently, it is also the most widely applied standard certification for testing the stability of

Please cite this article in press as: Lee et al., The Development of Transparent Photovoltaics, Cell Reports Physical Science (2020), https://doi.org/10.1016/j.xcrp.2020.100143

next-generation PV such as OPV, perovskite PV, and DSSC. The IEC 61646 standard comprises a set of tests elaborating the standard conditions and requirements for PV module certification, which are designed to test whether the PV module maintains its performance under prolonged exposure to standard climate conditions such as UV exposure and repeated temperature changes in the range of –40°C to 85°C at a relative humidity of 85%[118]

Because of harsh test conditions, three general phenomena designate "failure" in PV modules: (1) non-power generation (catastrophic, negligible output), (2) efficiency loss or lower power generation than the designed threshold value, and (3) issues caused by system instability. In particular, for the TPV module, aesthetic variations over the time period may be additionally considered as an important variable[119] The main causes of failure of thin-film PV modules are oxygen and humidity. Although the stability analysis of TPV modules has not been performed, it is evident that non-Si TPV modules would exhibit failures similar to those observed in conventional organic or perovskite thin-film PV modules[119] Oxygen can be photo-activated by UV light, and then super oxides and hydrogen peroxide can be generated, which degrade organic semiconductors in PV[120,121] In addition, air exposure affects the efficiency of the PV by diffusing water vapor as well as oxygen into the PV. In particular, for the perovskite PV, a photoactive material such as methyl-ammonium lead iodide is hydrolyzed in water, causing the decomposition of perovskite[122] Therefore, the encapsulation of the module is critical to fulfill requirements such as a water vapor transmission rate (WVTR) of 10^{-3}–10^{-6} $g \times m^{-2} \times day^{-1}$ and oxygen transmission rate (OTR) of 10^{-3}–10^{-5} $cm^3 \times m^{-2} \times day^{-1} \times atm^{-1}$[123] Although various materials, such as UV-cured epoxy[124] polyisobutylene[125] and atomic-layer-deposited alumina[126] have been applied to organic and perovskite PV as the encapsulating layer, the use of these materials with low WVTR and OTR would increase the cost. Accordingly, to commercialize a TPV module, it is necessary to develop a flexible, light, and inexpensive encapsulation material that is transparent to sunlight. For this, the high stability of the *c*-Si TPV, which are more stable in moisture and oxygen than the non-Si-based thin-film TPV, would increase the possibility of the commercialization of the TPV modules.

FUTURE OUTLOOK

Although TPV has been extensively researched as a renewable energy source for urban areas, a high-performance TPV cannot be realized commercially yet. For this, several key elements have been suggested in this review as important considerations for the development of TPV, including (1) a high PCE at the same AVT and minimization of the PCE degradation due to the angle of light incidence, (2) neutral color and low transmission haze ratio similar to glass, (3) modularization, and (4) high stability. Notably, each element must be verified through explicit evaluation standards. Among the TPV already developed, the best candidate for commercialization to satisfy these requirements is the *c*-Si TPV[3] Currently, *c*-Si TPV show a PCE of up to 12.2% (AVT of 20%), which is the highest among neutral-colored TPV. Further, the stability is expected to be the same as that of commercial *c*-Si PV. However, the unit cell must be scaled up to a size of over 5 inches, and research on modularization is required to produce the required current and voltage. In the modularization process, it is challenging to maintain the transparency of unit cells when connecting electrodes. Another way to develop a neutral-colored TPV is using LSC. Although the basic idea of LSC is clear and promising, further research is required to improve the PCE of the LSC-type neutral-colored TPV. However, large-sized LSC-type TPV would be easily fabricated by coating a luminescent material on a transparent

Please cite this article in press as: Lee et al., The Development of Transparent Photovoltaics, Cell Reports Physical Science (2020), https://doi.org/10.1016/j.xcrp.2020.100143

substrate; thus, it is considered as a potential technology that can replace the large glass windows of a building. In addition, if the LSC technology can be combined with other TPV technologies, the development of more advanced TPV may be possible. For example, if the LSC technology is applied to the LTW part of the *c*-Si TPV, the transmitted UV/NIR light through the LTW region is expected to be re-absorbed by the LSC. This re-absorption process would increase the PCE of the *c*-Si TPV while maintaining the neutral color and high transmittance of the device.

Another challenge in the commercialization of TPV is the angle dependency of the device. Since the position of the sun changes during the day and year, the PCE of PV also varies with time. In particular, because TPV would be installed in a fixed space with a relatively large angle to the sun, the cultivated energy may be much less than the expected value estimated under normal incidence condition. Therefore, a new strategy is required to minimize the PCE difference according to the angle of light incidence. A spherical PV is an example design that equalizes the amount of light entering the PV at all incident angles[127] In *c*-Si TPV, angled incident light can be absorbed through the wall of the LTW, reducing the PCE degradation according to the incident light angle[3] However, there are significantly fewer studies on limiting PCE degradation due to the angle of incident light compared with those on opaque PV. Therefore, further research for optimizing TPV is needed to minimize the PCE drop depending on the angle of the incident light.

The development of TPV will lead to commercialization, which will present a new paradigm to the PV market. When the windows of a building with a window-to-wall ratio of 55% is replaced with 30 W TPV (AVT of 15%), more than 40% of the energy consumed in the building can be generated from the PV[128] In addition, TPV could be applied to vehicles. On hot days, many dangerous situations occur due to an increase in the internal temperature of the car. In particular, a number of deaths of children or pets are reported every year due to the rising temperature inside parked vehicles[129] If TPV is applied to cars, these dangerous situations can be prevented by lowering the temperature inside the car by operating the electric fan on hot days, even when the engine of the vehicle is off[130] Another example is applying TPV to greenhouses. This will enable the building of smart farm systems that automatically check and regulate plant conditions, temperature, and humidity through a self-powered Internet of Things (IoT) system powered by the TPV. As such, the commercialization of TPV is expected to foster new types of industries beyond simply expanding the applicable space of PV.

ACKNOWLEDGMENTS

This work was supported by the New Renewable Energy Core Technology Development Project of the Korea Institute of Energy Technology Evaluation and Planning (KETEP) granted financial resource from the Ministry of Trade, Industry & Energy, Republic of Korea (No. 20183010013900). It was also supported by the National Research Foundation of Korea (NRF) grant funded by the Korean Government (MSIP) (NRF-2019R1A2C2086602, NRF-2019M1A2A2065614, NRF-2017M1A2A2087812, and 2016K1A4A4A01922028). This work also was supported by the 2020 Research Fund (1.200070.01) of UNIST (Ulsan National Institute of Science & Technology).

AUTHOR CONTRIBUTIONS

K.S. proposed the topic. K.L. and K.S. organized the manuscript. All authors contributed to the discussion and completion of the manuscript.

DECLARATION OF INTERESTS

The authors declare no competing interests.

REFERENCES

1. Heinstein, P., Ballif, C., and Perret-Aebi, L.-E. (2013). Building integrated photovoltaics (BIPV): review, potentials, barriers and myths. Green *3*, 125–156.
2. Della Gaspera, E., Peng, Y., Hou, Q., Spiccia, L., Bach, U., Jasieniak, J.J., and Cheng, Y.-B. (2015). Ultra-thin high efficiency semitransparent perovskite solar cells. Nano Energy *13*, 249–257.
3. Lee, K., Kim, N., Kim, K., Um, H.-D., Jin, W., Choi, D., Park, J., Park, K.J., Lee, S., and Seo, K. (2020). Neutral-Colored Transparent Crystalline Silicon Photovoltaics. Joule *4*, 235–246.
4. Zhao, Y., Meek, G.A., Levine, B.G., and Lunt, R.R. (2014). Near-infrared harvesting transparent luminescent solar concentrators. Adv. Opt. Mater. *2*, 606–611.
5. Xue, Q., Bai, Y., Liu, M., Xia, R., Hu, Z., Chen, Z., Jiang, X.F., Huang, F., Yang, S., and Matsuo, Y. (2017). Dual interfacial modifications enable high performance semitransparent perovskite solar cells with large open circuit voltage and fill factor. Adv. Energy Mater. *7*, 1602333.
6. Yang, C., Moemeni, M., Bates, M., Sheng, W., Borhan, B., and Lunt, R.R. (2020). High-Performance Near-Infrared Harvesting Transparent Luminescent Solar Concentrators. Adv. Opt. Mater. *8*, 1901536.
7. Green, M.A., Dunlop, E.D., Hohl-Ebinger, J., Yoshita, M., Kopidakis, N., and Ho-Baillie, A.W. (2019). Solar cell efficiency tables (version 55). Prog. Photovolt. Res. Appl. Published online 20 December 2019. https://doi.org/10.1002/pip.3228.
8. Colonna, D., Capogna, V., Lembo, A., Brown, T.M., Reale, A., and Di Carlo, A. (2012). Efficient cosensitization strategy for dye-sensitized solar cells. Appl. Phys. Express *5*, 022303.
9. Saifullah, M., Gwak, J., and Yun, J.H. (2016). Comprehensive review on material requirements, present status, and future prospects for building-integrated semitransparent photovoltaics (BISTPV). J. Mater. Chem. A Mater. Energy Sustain. *4*, 8512–8540.
10. Wen, L., Chen, Q., Sun, F., Song, S., Jin, L., and Yu, Y. (2014). Theoretical design of multi-colored semi-transparent organic solar cells with both efficient color filtering and light harvesting. Sci. Rep. *4*, 7036.
11. Liu, Z., You, P., Liu, S., and Yan, F. (2015). Neutral-color semitransparent organic solar cells with all-graphene electrodes. ACS Nano *9*, 12026–12034.
12. Xue, Q., Xia, R., Brabec, C.J., and Yip, H.-L. (2018). Recent advances in semi-transparent polymer and perovskite solar cells for power generating window applications. Energy Environ. Sci. *11*, 1688–1709.
13. Xiong, Z., Walsh, T.M., and Aberle, A.G. (2011). PV module durability testing under high voltage biased damp heat conditions. Energy Procedia *8*, 384–389.
14. Burlingame, Q., Huang, X., Liu, X., Jeong, C., Coburn, C., and Forrest, S.R. (2019). Intrinsically stable organic solar cells under high-intensity illumination. Nature *573*, 394–397.
15. Traverse, C.J., Chen, P., and Lunt, R.R. (2018). Lifetime of organic salt photovoltaics. Adv. Energy Mater. *8*, 1703678.
16. Jørgensen, M., Norrman, K., Gevorgyan, S.A., Tromholt, T., Andreasen, B., and Krebs, F.C. (2012). Stability of polymer solar cells. Adv. Mater. *24*, 580–612.
17. Mozaffari, S., Nateghi, M.R., and Zarandi, M.B. (2017). An overview of the Challenges in the commercialization of dye sensitized solar cells. Renew. Sustain. Energy Rev. *71*, 675–686.
18. Wang, R., Mujahid, M., Duan, Y., Wang, Z.K., Xue, J., and Yang, Y. (2019). A review of perovskites solar cell stability. Adv. Funct. Mater. *29*, 1808843.
19. Louwen, A., Van Sark, W., Schropp, R., and Faaij, A. (2016). A cost roadmap for silicon heterojunction solar cells. Sol. Energy Mater. Sol. Cells *147*, 295–314.
20. Chang, N.L., Yi Ho-Baillie, A.W., Basore, P.A., Young, T.L., Evans, R., and Egan, R.J. (2017). A manufacturing cost estimation method with uncertainty analysis and its application to perovskite on glass photovoltaic modules. Prog. Photovolt. Res. Appl. *25*, 390–405.
21. Kalowekamo, J., and Baker, E. (2009). Estimating the manufacturing cost of purely organic solar cells. Sol. Energy *83*, 1224–1231.
22. Kirchartz, T. (2019). High open-circuit voltages in lead-halide perovskite solar cells: experiment, theory and open questions. Philos. Trans.- Royal Soc., Math. Phys. Eng. Sci. *377*, 20180286.
23. Beiley, Z.M., Christoforo, M.G., Gratia, P., Bowring, A.R., Eberspacher, P., Margulis, G.Y., Cabanetos, C., Beaujuge, P.M., Salleo, A., and McGehee, M.D. (2013). Semi-transparent polymer solar cells with excellent sub-bandgap transmission for third generation photovoltaics. Adv. Mater. *25*, 7020–7026.
24. Selvaraj, P., Baig, H., Mallick, T.K., Siviter, J., Montecucco, A., Li, W., Paul, M., Sweet, T., Gao, M., and Knox, A.R. (2018). Enhancing the efficiency of transparent dye-sensitized solar cells using concentrated light. Sol. Energy Mater. Sol. Cells *175*, 29–34.
25. Shin, M.J., Jo, J.H., Cho, A., Gwak, J., Yun, J.H., Kim, K., Ahn, S.K., Park, J.H., Yoo, J., and Jeong, I. (2019). Semi-transparent photovoltaics using ultra-thin Cu (In, Ga) Se2 absorber layers prepared by single-stage co-evaporation. Sol. Energy *181*, 276–284.
26. Yang, R., Lee, C.-H., Cui, B., and Sazonov, A. (2018). Flexible semi-transparent a-Si: H pin solar cells for functional energy-harvesting applications. Mater. Sci. Eng. B *229*, 1–5.
27. Alrashidi, H., Ghosh, A., Issa, W., Sellami, N., Mallick, T.K., and Sundaram, S. (2020). Thermal performance of semitransparent CdTe BIPV window at temperate climate. Sol. Energy *195*, 536–543.
28. Zhang, X., Hägglund, C., and Johansson, E.M. (2017). Highly efficient, transparent and stable semitransparent colloidal quantum dot solar cells: a combined numerical modeling and experimental approach. Energy Environ. Sci. *10*, 216–224.
29. Heo, J.H., Han, H.J., Lee, M., Song, M., Kim, D.H., and Im, S.H. (2015). Stable semi-transparent CH 3 NH 3 PbI 3 planar sandwich solar cells. Energy Environ. Sci. *8*, 2922–2927.
30. Habibi, M., Zabihi, F., Ahmadian-Yazdi, M.R., and Eslamian, M. (2016). Progress in emerging solution-processed thin film solar cells–Part II: Perovskite solar cells. Renew. Sustain. Energy Rev. *62*, 1012–1031.
31. Lim, J.W., Kim, G., Shin, M., and Yun, S.J. (2017). Colored a-Si: H transparent solar cells employing ultrathin transparent multi-layered electrodes. Sol. Energy Mater. Sol. Cells *163*, 164–169.
32. Lim, J.W., Shin, M., Lee, S.H., and Yun, S.J. (2014). Highly transparent amorphous silicon solar cells fabricated using thin absorber and high-bandgap-energy n/i-interface layers. Sol. Energy Mater. Sol. Cells *128*, 301–306.
33. Myong, S.Y., and Jeon, S.W. (2015). Design of esthetic color for thin-film silicon semi-transparent photovoltaic modules. Sol. Energy Mater. Sol. Cells *143*, 442–449.
34. Choi, S.-W., Yang, J., Park, J.-H., Han, S.-J., Song, P., Kang, D.-W., and Kwon, J.-D. (2019). P/i interfacial engineering in semi-transparent silicon thin film solar cells for fabrication at a low temperature of 150° C. Curr. Appl. Phys. *19*, 1120–1126.
35. Saifullah, M., Ahn, S., Gwak, J., Ahn, S., Kim, K., Cho, J., Park, J.H., Eo, Y.J., Cho, A., and Yoo, J.-S. (2016). Development of semitransparent CIGS thin-film solar cells modified with a sulfurized-AgGa layer for building applications. J. Mater. Chem. A Mater. Energy Sustain. *4*, 10542–10551.
36. Mutalikdesai, A., and Ramasesha, S.K. (2017). Solution process for fabrication of thin film CdS/CdTe photovoltaic cell for building integration. Thin Solid Films *632*, 73–78.
37. Tavakoli Dastjerdi, H., Qi, P., Fan, Z., and Tavakoli, M.M. (2020). Cost-Effective and Semi-Transparent PbS Quantum Dot Solar Cells Using Copper Electrodes. ACS Appl. Mater. Interfaces *12*, 818–825.

38. Yin, Z., Wei, J., Chen, S.-C., Cai, D., Ma, Y., Wang, M., and Zheng, Q. (2017). Long lifetime stable and efficient semitransparent organic solar cells using a ZnMgO-modified cathode combined with a thin MoO 3/Ag anode. J. Mater. Chem. A Mater. Energy Sustain. *5*, 3888–3899.

39. Wong, Y.Q., Meng, H.-F., Wong, H.Y., Tan, C.S., Wu, C.-Y., Tsai, P.-T., Chang, C.-Y., Horng, S.-F., and Zan, H.-W. (2017). Efficient semitransparent organic solar cells with good color perception and good color rendering by blade coating. Org. Electron. *43*, 196–206.

40. Zhang, Y., Peng, Z., Cai, C., Liu, Z., Lin, Y., Zheng, W., Yang, J., Hou, L., and Cao, Y. (2016). Colorful semitransparent polymer solar cells employing a bottom periodic one-dimensional photonic crystal and a top conductive PEDOT: PSS layer. J. Mater. Chem. A Mater. Energy Sustain. *4*, 11821–11828.

41. Song, Y., Chang, S., Gradecak, S., and Kong, J. (2016). Visibly-transparent organic solar cells on flexible substrates with all-graphene electrodes. Adv. Energy Mater. *6*, 1600847.

42. Min, J., Bronnbauer, C., Zhang, Z.G., Cui, C., Luponosov, Y.N., Ata, I., Schweizer, P., Przybilla, T., Guo, F., and Ameri, T. (2016). Fully Solution-Processed Small Molecule Semitransparent Solar Cells: Optimization of Transparent Cathode Architecture and Four Absorbing Layers. Adv. Funct. Mater. *26*, 4543–4550.

43. Xu, G., Shen, L., Cui, C., Wen, S., Xue, R., Chen, W., Chen, H., Zhang, J., Li, H., and Li, Y. (2017). High-performance colorful semitransparent polymer solar cells with ultrathin hybrid-metal electrodes and fine-tuned dielectric mirrors. Adv. Funct. Mater. *27*, 1605908.

44. Upama, M.B., Wright, M., Elumalai, N.K., Mahmud, M.A., Wang, D., Chan, K.H., Xu, C., Haque, F., and Uddin, A. (2017). High performance semitransparent organic solar cells with 5% PCE using non-patterned MoO3/Ag/MoO3 anode. Curr. Appl. Phys. *17*, 298–305.

45. Hu, Z., Wang, J., Wang, Z., Gao, W., An, Q., Zhang, M., Ma, X., Wang, J., Miao, J., and Yang, C. (2019). Semitransparent ternary nonfullerene polymer solar cells exhibiting 9.40% efficiency and 24.6% average visible transmittance. Nano Energy *55*, 424–432.

46. Li, X., Meng, H., Shen, F., Su, D., Huo, S., Shan, J., Huang, J., and Zhan, C. (2019). Semitransparent fullerene-free polymer solar cell with 44% AVT and 7% efficiency based on a new chlorinated small molecule acceptor. Dyes Pigments *166*, 196–202.

47. Sun, G., Shahid, M., Fei, Z., Xu, S., Eisner, F.D., Anthopolous, T.D., McLachlan, M.A., and Heeney, M. (2019). Highly-efficient semi-transparent organic solar cells utilising non-fullerene acceptors with optimised multilayer MoO3/Ag/MoO3 electrodes. Mater. Chem. Front. *3*, 450–455.

48. López-López, C., Colodrero, S., and Míguez, H. (2014). Panchromatic porous specular back reflectors for efficient transparent dye solar cells. Phys. Chem. Chem. Phys. *16*, 663–668.

49. Passoni, L., Fumagalli, F., Perego, A., Bellani, S., Mazzolini, P., and Di Fonzo, F. (2017). Multi-layered hierarchical nanostructures for transparent monolithic dye-sensitized solar cell architectures. Nanotechnology *28*, 245603.

50. Li, F., Xu, Y., Chen, W., Xie, S., and Li, J. (2017). Nanotube enhanced carbon grids as top electrodes for fully printable mesoscopic semitransparent perovskite solar cells. J. Mater. Chem. A Mater. Energy Sustain. *5*, 10374–10379.

51. Kwon, H.C., Kim, A., Lee, H., Lee, D., Jeong, S., and Moon, J. (2016). Parallelized nanopillar perovskites for semitransparent solar cells using an anodized aluminum oxide scaffold. Adv. Energy Mater. *6*, 1601055.

52. Bag, S., and Durstock, M.F. (2016). Efficient semi-transparent planar perovskite solar cells using a 'molecular glue'. Nano Energy *30*, 542–548.

53. Kim, H., Kim, H.S., Ha, J., Park, N.G., and Yoo, S. (2016). Empowering semi-transparent solar cells with thermal-mirror functionality. Adv. Energy Mater. *6*, 1502466.

54. Lee, H.-J., Cho, S.-P., Na, S.-i., and Kim, S.-S. (2019). Thin metal top electrode and interface engineering for efficient and air-stable semitransparent perovskite solar cells. J. Alloys Compd. *797*, 65–73.

55. Islam, M.B., Yanagida, M., Shirai, Y., Nabetani, Y., and Miyano, K. (2019). Highly stable semi-transparent MAPbI3 perovskite solar cells with operational output for 4000 h. Sol. Energy Mater. Sol. Cells *195*, 323–329.

56. Xiao, S., Chen, H., Jiang, F., Bai, Y., Zhu, Z., Zhang, T., Zheng, X., Qian, G., Hu, C., and Zhou, Y. (2016). Hierarchical Dual-Scaffolds Enhance Charge Separation and Collection for High Efficiency Semitransparent Perovskite Solar Cells. Adv. Mater. Interfaces *3*, 1600484.

57. Yang, C., Liu, D., Bates, M., Barr, M.C., and Lunt, R.R. (2019). How to accurately report transparent solar cells. Joule *3*, 1803–1809.

58. Rowell, M.W., and McGehee, M.D. (2011). Transparent electrode requirements for thin film solar cell modules. Energy Environ. Sci. *4*, 131–134.

59. Hunger, C., Rao, K., Gupta, R., Singh, C.R., Kulkarni, G.U., and Thelakkat, M. (2015). Transparent Metal Network with Low Haze and High Figure of Merit applied to Front and Back Electrodes in Semitransparent ITO-free Polymer Solar Cells. Energy Technol. (Weinheim) *3*, 638–645.

60. Fang, Y., Wu, Z., Li, J., Jiang, F., Zhang, K., Zhang, Y., Zhou, Y., Zhou, J., and Hu, B. (2018). High-Performance Hazy Silver Nanowire Transparent Electrodes through Diameter Tailoring for Semitransparent Photovoltaics. Adv. Funct. Mater. *28*, 1705409.

61. Bryant, D., Greenwood, P., Troughton, J., Wijdekop, M., Carnie, M., Davies, M., Wojciechowski, K., Snaith, H.J., Watson, T., and Worsley, D. (2014). A transparent conductive adhesive laminate electrode for high-efficiency organic-inorganic lead halide perovskite solar cells. Adv. Mater. *26*, 7499–7504.

62. Sohn, H., Park, C., Oh, J.-M., Kang, S.W., and Kim, M.-J. (2019). Silver nanowire networks: Mechano-electric properties and applications. Materials (Basel) *12*, 2526.

63. Bolotin, K.I., Sikes, K.J., Jiang, Z., Klima, M., Fudenberg, G., Hone, J., Kim, P., and Stormer, H. (2008). Ultrahigh electron mobility in suspended graphene. Solid State Commun. *146*, 351–355.

64. Serway, R.A. (1998). Principles of Physics (Saunders College Pub).

65. Hu, L., Kim, H.S., Lee, J.-Y., Peumans, P., and Cui, Y. (2010). Scalable coating and properties of transparent, flexible, silver nanowire electrodes. ACS Nano *4*, 2955–2963.

66. Um, H.D., Hwang, I., Kim, N., Yu, Y.J., Wober, M., Kim, K.H., and Seo, K. (2015). Microgrid electrode for Si microwire solar cells with a fill factor of over 80%. Adv. Mater. Interfaces *2*, 1500347.

67. Peng, C., Huang, Y., and Wu, Z. (2011). Building-integrated photovoltaics (BIPV) in architectural design in China. Energy Build. *43*, 3592–3598.

68. Yoon, J., Baca, A.J., Park, S.-I., Elvikis, P., Geddes, J.B., 3rd, Li, L., Kim, R.H., Xiao, J., Wang, S., Kim, T.-H., et al. (2008). Ultrathin silicon solar microcells for semitransparent, mechanically flexible and microconcentrator module designs. Nat. Mater. *7*, 907–915.

69. Yano, A., Onoe, M., and Nakata, J. (2014). Prototype semi-transparent photovoltaic modules for greenhouse roof applications. Biosyst. Eng. *122*, 62–73.

70. Takeoka, A., Kouzuma, S., Tanaka, H., Inoue, H., Murata, K., Morizane, M., Nakamura, N., Nishiwaki, H., Ohnishi, M., and Nakano, S. (1993). Development and application of see-through a-Si solar cells. Sol. Energy Mater. Sol. Cells *29*, 243–252.

71. Fath, P., Nussbaumer, H., and Burkhardt, R. (2002). Industrial manufacturing of semitransparent crystalline silicon POWER solar cells. Sol. Energy Mater. Sol. Cells *74*, 127–131.

72. Ordy, J.M., Latanick, A., Samorajki, T., and Massopust, L.C., Jr. (1964). Visual Acuity in Newborn Primate Infants. Proc. Soc. Exp. Biol. Med. *115*, 677–680.

73. Pastorelli, F., Romero-Gomez, P., Betancur, R., Martinez-Otero, A., Mantilla-Perez, P., Bonod, N., and Martorell, J. (2015). Enhanced light harvesting in semitransparent organic solar cells using an optical metal cavity configuration. Adv. Energy Mater. *5*, 1400614.

74. Yu, W., Jia, X., Long, Y., Shen, L., Liu, Y., Guo, W., and Ruan, S. (2015). Highly efficient semitransparent polymer solar cells with color rendering index approaching 100 using one-dimensional photonic crystal. ACS Appl. Mater. Interfaces *7*, 9920–9928.

75. Chen, C.-C., Dou, L., Gao, J., Chang, W.-H., Li, G., and Yang, Y. (2013). High-performance semi-transparent polymer solar cells possessing tandem structures. Energy Environ. Sci. *6*, 2714–2720.

76. Wang, W., Yan, C., Lau, T.K., Wang, J., Liu, K., Fan, Y., Lu, X., and Zhan, X. (2017). Fused

hexacyclic nonfullerene acceptor with strong near-infrared absorption for semitransparent organic solar cells with 9.77% efficiency. Adv. Mater. *29*, 1701308.

77. Meiss, J., Menke, T., Leo, K., Uhrich, C., Gnehr, W.-M., Sonntag, S., Pfeiffer, M., and Riede, M. (2011). Highly efficient semitransparent tandem organic solar cells with complementary absorber materials. Appl. Phys. Lett. *99*, 143.

78. Zhang, K., Qin, C., Yang, X., Islam, A., Zhang, S., Chen, H., and Han, L. (2014). High-Performance, Transparent, Dye-Sensitized Solar Cells for See-Through Photovoltaic Windows. Adv. Energy Mater. *4*, 1301966.

79. Lin, H.-W., Chen, Y.-H., Huang, Z.-Y., Chen, C.-W., Lin, L.-Y., Lin, F., and Wong, K.-T. (2012). Highly efficient bifacial transparent organic solar cells with power conversion efficiency greater than 3% and transparency of 50%. Org. Electron. *13*, 1722–1728.

80. Meiss, J., Holzmueller, F., Gresser, R., Leo, K., and Riede, M. (2011). Near-infrared absorbing semitransparent organic solar cells. Appl. Phys. Lett. *99*, 252.

81. Xiao, X., Lee, K., and Forrest, S.R. (2015). Inverted, semitransparent small molecule photovoltaic cells. Appl. Phys. Lett. *107*, 033901.

82. Véron, A.C., Zhang, H., Linden, A., Nüesch, F., Heier, J., Hany, R., and Geiger, T. (2014). NIR-absorbing heptamethine dyes with tailor-made counterions for application in light to energy conversion. Org. Lett. *16*, 1044–1047.

83. Liu, F., Zhou, Z., Zhang, C., Zhang, J., Hu, Q., Vergote, T., Liu, F., Russell, T.P., and Zhu, X. (2017). Efficient semitransparent solar cells with high NIR responsiveness enabled by a small-bandgap electron acceptor. Adv. Mater. *29*, 1606574.

84. Zhang, H., Wicht, G., Gretener, C., Nagel, M., Nüesch, F., Romanyuk, Y., Tisserant, J.-N., and Hany, R. (2013). Semitransparent organic photovoltaics using a near-infrared absorbing cyanine dye. Sol. Energy Mater. Sol. Cells *118*, 157–164.

85. Chen, C.-C., Dou, L., Zhu, R., Chung, C.-H., Song, T.-B., Zheng, Y.B., Hawks, S., Li, G., Weiss, P.S., and Yang, Y. (2012). Visibly transparent polymer solar cells produced by solution processing. ACS Nano *6*, 7185–7190.

86. Yang, C., and Lunt, R.R. (2017). Limits of visibly transparent luminescent solar concentrators. Adv. Opt. Mater. *5*, 1600851.

87. Kim, H.-T., Lee, K., Jin, W., Um, H.-D., Lee, M., Hwang, E., Kwon, T.-H., and Seo, K. (2018). Phosphorescent Energy Downshifting for Diminishing Surface Recombination in Silicon Nanowire Solar Cells. Sci. Rep. *8*, 16974.

88. van Sark, W.G., Barnham, K.W., Slooff, L.H., Chatten, A.J., Büchtemann, A., Meyer, A., McCormack, S.J., Koole, R., Farrell, D.J., Bose, R., et al. (2008). Luminescent Solar Concentrators–a review of recent results. Opt. Express *16*, 21773–21792.

89. Meinardi, F., Ehrenberg, S., Dhamo, L., Carulli, F., Mauri, M., Bruni, F., Simonutti, R., Kortshagen, U., and Brovelli, S. (2017). Highly efficient luminescent solar concentrators based on earth-abundant indirect-bandgap silicon quantum dots. Nat. Photonics *11*, 177.

90. Coropceanu, I., and Bawendi, M.G. (2014). Core/shell quantum dot based luminescent solar concentrators with reduced reabsorption and enhanced efficiency. Nano Lett. *14*, 4097–4101.

91. Traverse, C.J., Pandey, R., Barr, M.C., and Lunt, R.R. (2017). Emergence of highly transparent photovoltaics for distributed applications. Nat. Energy *2*, 849.

92. Sutherland, B.R. (2018). Cost competitive luminescent solar concentrators. Joule *2*, 203–204.

93. Meinardi, F., Bruni, F., and Brovelli, S. (2017). Luminescent solar concentrators for building-integrated photovoltaics. Nat. Rev. Mater. *2*, 1–9.

94. Zhao, Y., and Lunt, R.R. (2013). Transparent Luminescent Solar Concentrators for Large-Area Solar Windows Enabled by Massive Stokes-Shift Nanocluster Phosphors. Adv. Energy Mater. *3*, 1143–1148.

95. Yang, C., Liu, D., Renny, A., Kuttipillai, P.S., and Lunt, R.R. (2019). Integration of near-infrared harvesting transparent luminescent solar concentrators onto arbitrary surfaces. J. Lumin. *210*, 239–246.

96. Banal, J.L., White, J.M., Lam, T.W., Blakers, A.W., Ghiggino, K.P., and Wong, W.W. (2015). A Transparent Planar Concentrator Using Aggregates of gem-Pyrene Ethenes. Adv. Energy Mater. *5*, 1500818.

97. Wang, T., Zhang, J., Ma, W., Luo, Y., Wang, L., Hu, Z., Wu, W., Wang, X., Zou, G., and Zhang, Q. (2011). Luminescent solar concentrator employing rare earth complex with zero self-absorption loss. Sol. Energy *85*, 2571–2579.

98. Erickson, C.S., Bradshaw, L.R., McDowall, S., Gilbertson, J.D., Gamelin, D.R., and Patrick, D.L. (2014). Zero-reabsorption doped-nanocrystal luminescent solar concentrators. ACS Nano *8*, 3461–3467.

99. Zhao, H., Benetti, D., Jin, L., Zhou, Y., Rosei, F., and Vomiero, A. (2016). Absorption Enhancement in "Giant" Core/Alloyed-Shell Quantum Dots for Luminescent Solar Concentrator. Small *12*, 5354–5365.

100. Bradshaw, L.R., Knowles, K.E., McDowall, S., and Gamelin, D.R. (2015). Nanocrystals for luminescent solar concentrators. Nano Lett. *15*, 1315–1323.

101. Zhou, Y., Benetti, D., Fan, Z., Zhao, H., Ma, D., Govorov, A.O., Vomiero, A., and Rosei, F. (2016). Near infrared, highly efficient luminescent solar concentrators. Adv. Energy Mater. *6*, 1501913.

102. Sanguineti, A., Monguzzi, A., Vaccaro, G., Meinardi, F., Ronchi, E., Moret, M., Cosentino, U., Moro, G., Simonutti, R., Mauri, M., et al. (2012). NIR emitting ytterbium chelates for colourless luminescent solar concentrators. Phys. Chem. Chem. Phys. *14*, 6452–6455.

103. Berends, A.C., Rabouw, F.T., Spoor, F.C., Bladt, E., Grozema, F.C., Houtepen, A.J., Siebbeles, L.D., and de Mello Donegá, C. (2016). Radiative and nonradiative recombination in CuInS2 nanocrystals and CuInS2-based core/shell nanocrystals. J. Phys. Chem. Lett. *7*, 3503–3509.

104. Li, C., Chen, W., Wu, D., Quan, D., Zhou, Z., Hao, J., Qin, J., Li, Y., He, Z., and Wang, K. (2015). Large Stokes shift and high efficiency luminescent solar concentrator incorporated with CuInS 2/ZnS quantum dots. Sci. Rep. *5*, 17777.

105. Mateker, W.R., Sachs-Quintana, I., Burkhard, G.F., Cheacharoen, R., and McGehee, M.D. (2015). Minimal long-term intrinsic degradation observed in a polymer solar cell illuminated in an oxygen-free environment. Chem. Mater. *27*, 404–407.

106. Campbell, P., and Green, M.A. (1986). The limiting efficiency of silicon solar cells under concentrated sunlight. IEEE Trans. Electron Dev. *33*, 234–239.

107. Yang, C., Liu, D., and Lunt, R.R. (2019). How to Accurately Report Transparent Luminescent Solar Concentrators. Joule *3*, 2871–2876.

108. Yaghoubi, H., Lafalce, E., Jun, D., Jiang, X., Beatty, J.T., and Takshi, A. (2015). Large photocurrent response and external quantum efficiency in biophotoelectrochemical cells incorporating reaction center plus light harvesting complexes. Biomacromolecules *16*, 1112–1118.

109. Tai, Q., and Yan, F. (2017). Emerging semitransparent solar cells: materials and device design. Adv. Mater. *29*, 1700192.

110. Zimmermann, E., Ehrenreich, P., Pfadler, T., Dorman, J.A., Weickert, J., and Schmidt-Mende, L. (2014). Erroneous efficiency reports harm organic solar cell research. Nat. Photonics *8*, 669.

111. Hwang, I., Choi, D., Lee, S., Seo, J.H., Kim, K.-H., Yoon, I., and Seo, K. (2017). Enhancement of light absorption in photovoltaic devices using textured polydimethylsiloxane stickers. ACS Appl. Mater. Interfaces *9*, 21276–21282.

112. Tang, Y., Cai, W., and Xu, B. (2015). Profiles of phenolics, carotenoids and antioxidative capacities of thermal processed white, yellow, orange and purple sweet potatoes grown in Guilin, China. Food Sci. Hum. Wellness *4*, 123–132.

113. Leon, K., Mery, D., Pedreschi, F., and Leon, J. (2006). Color measurement in L* a* b* units from RGB digital images. Food Res. Int. *39*, 1084–1091.

114. Yang, H.E., French, R., and Bruckman, L. (2019). Durability and Reliability of Polymers and Other Materials in Photovoltaic Modules (William Andrew).

115. Yoshikawa, K., Kawasaki, H., Yoshida, W., Irie, T., Konishi, K., Nakano, K., Uto, T., Adachi, D., Kanematsu, M., and Uzu, H. (2017). Silicon heterojunction solar cell with interdigitated back contacts for a photoconversion efficiency over 26%. Nat. Energy *2*, 17032.

116. Kurinec, S.K. (2018). Emerging Photovoltaic Materials: Silicon & Beyond (John Wiley & Sons).

117. Pern, F. (1997). Ethylene-vinyl acetate (EVA) encapsulants for photovoltaic modules:

Degradation and discoloration mechanisms and formulation modifications for improved photostability. Die Angewandte Makromolekulare Chemie: Applied Macromolecular Chemistry and Physics *252*, 195–216.

118. Arndt, R., and Puto, R. (2010). Basic Understanding of IEC Standard Testing for Photovoltaic Panels (Compliance Magazine).

119. Roesch, R., Faber, T., Von Hauff, E., Brown, T.M., Lira-Cantu, M., and Hoppe, H. (2015). Procedures and Practices for Evaluating Thin-Film Solar Cell Stability. Adv. Energy Mater. *5*, 1501407.

120. Madsen, M.V., Norrman, K., and Krebs, F.C. (2011). Oxygen-and water-induced degradation of an inverted polymer solar cell: the barrier effect. Journal of Photonics for Energy *1*, 011104.

121. Neugebauer, H., Brabec, C., Hummelen, J., and Sariciftci, N. (2000). Stability and photodegradation mechanisms of conjugated polymer/fullerene plastic solar cells. Sol. Energy Mater. Sol. Cells *61*, 35–42.

122. Niu, G., Guo, X., and Wang, L. (2015). Review of recent progress in chemical stability of perovskite solar cells. J. Mater. Chem. A Mater. Energy Sustain. *3*, 8970–8980.

123. Kang, H., Kim, G., Kim, J., Kwon, S., Kim, H., and Lee, K. (2016). Bulk-heterojunction organic solar cells: five core technologies for their commercialization. Adv. Mater. *28*, 7821–7861.

124. Dong, Q., Liu, F., Wong, M.K., Tam, H.W., Djurišić, A.B., Ng, A., Surya, C., Chan, W.K., and Ng, A.M.C. (2016). Encapsulation of perovskite solar cells for high humidity conditions. ChemSusChem *9*, 2597–2603.

125. Shi, L., Young, T.L., Kim, J., Sheng, Y., Wang, L., Chen, Y., Feng, Z., Keevers, M.J., Hao, X., Verlinden, P.J., et al. (2017). Accelerated lifetime testing of organic–inorganic perovskite solar cells encapsulated by polyisobutylene. ACS Appl. Mater. Interfaces *9*, 25073–25081.

126. Choi, E.Y., Kim, J., Lim, S., Han, E., Ho-Baillie, A.W., and Park, N. (2018). Enhancing stability for organic-inorganic perovskite solar cells by atomic layer deposited Al2O3 encapsulation. Sol. Energy Mater. Sol. Cells *188*, 37–45.

127. Taira, K., and Nakata, J. (2010). Silicon cells: catching rays. Nat. Photonics *4*, 602.

128. Olivieri, L., Caamaño-Martín, E., Moralejo-Vázquez, F., Martín-Chivelet, N., Olivieri, F., and Neila-Gonzalez, F. (2014). Energy saving potential of semi-transparent photovoltaic elements for building integration. Energy *76*, 572–583.

129. Horak, J., Schmerold, I., Wimmer, K., and Schauberger, G. (2017). Cabin air temperature of parked vehicles in summer conditions: life-threatening environment for children and pets calculated by a dynamic model. Theor. Appl. Climatol. *130*, 107–118.

130. Dadour, I.R., Almanjahie, I., Fowkes, N.D., Keady, G., and Vijayan, K. (2011). Temperature variations in a parked vehicle. Forensic Sci. Int. *207*, 205–211.